Condensin I^{DC}, H4K20me1, and perinuclear tethering maintain X chromosome repression in *C. elegans*

Jessica Trombley, Audry I. Rakozy, Christian A. McClear, Eshna Jash, Györgyi Csankovszki*

Department of Molecular, Cellular, and Developmental Biology, University of Michigan, Ann Arbor, Michigan, United States of America

*corresponding author

e-mail: gyorgyi@umich.edu

Abstract

Dosage compensation in *Caenorhabditis elegans* equalizes X-linked gene expression between XX hermaphrodites and XO males. The process depends on a condensin-containing dosage compensation complex (DCC), which binds the X chromosomes in hermaphrodites to repress gene expression. Condensin I^{DC} and an additional five DCC components must be present on the X during early embryogenesis in hermaphrodites to establish dosage compensation. However, whether the DCC's continued presence is required to maintain the repressed state once established is unknown. Beyond the role of condensin I^{DC} in X chromosome compaction, additional mechanisms contribute to X-linked gene repression. DPY-21, a non-condensin I^{DC} DCC component, is an H4K20me2/3 demethylase whose activity enriches the repressive histone mark, H4 lysine 20 monomethylation, on the X chromosomes. In addition, CEC-4 tethers H3K9me3-rich chromosomal regions to the nuclear lamina, which also contributes to X-linked gene repression. To investigate the necessity of condensin I^{DC} during the larval and adult stages of hermaphrodites, we used the auxin-inducible degradation system to deplete the condensin I^{DC} subunit DPY-27. While DPY-27 depletion in the embryonic stages resulted in lethality, DPY-27 depleted larvae and adults survive. In these DPY-27 depleted strains, condensin I^{DC} was no longer associated with the X chromosome, the X became decondensed, and the H4K20me1 mark was gradually lost, leading to X-linked gene derepression. These results suggest that the stable maintenance of dosage compensation requires the continued presence of condensin I^{DC}. A loss-of-function mutation in *cec-4*, in addition to the depletion of DPY-27 or the genetic mutation of *dpy-21*, led to even more significant increases in X-linked gene expression, suggesting that tethering heterochromatic regions to the nuclear lamina helps stabilize repression mediated by condensin I^{DC} and H4K20me1.

Author Summary

In some organisms, whether an individual becomes male, female, or hermaphrodite is determined by the number of their sex chromosomes. In the nematode *Caenorhabditis elegans*, males have one X chromosome, whereas hermaphrodites have two X chromosomes. This difference in the number of X chromosomes is crucial for deciding whether an individual becomes a hermaphrodite or a male. However, having two X chromosomes can lead to problems because it results in different gene expression levels, resulting in hermaphrodite lethality. To solve this issue, many organisms undergo a process called dosage compensation. Dosage compensation in *C. elegans* is achieved by a group of proteins known as the dosage compensation complex (DCC), which includes a protein called DPY-27. The function of DPY-27 is essential during early embryonic development. This study shows that in contrast to early embryonic development, larvae and adults can still survive when DPY-27 is missing. In these worms, all known mechanisms involved in dosage compensation are disrupted and the X is no longer repressed. Our results suggest that the maintenance of dosage compensation in nematodes is an active process, and that it is essential for survival

when the organism is developing, but once fully developed, the process becomes dispensable.

Introduction

Chromosome conformation, subnuclear localization, and the post-translational modifications of histones are closely linked to gene expression. The relationship between these processes plays a crucial role in an organism's development, growth, and survival. Dosage compensation in the nematode *Caenorhabditis elegans* offers an excellent paradigm for exploring chromosome-wide gene regulation.

There is an inherent imbalance in chromosomal gene expression in species with heterogametic sexes [1]. As in numerous other species with chromosome-based sex determination, *C. elegans* has evolved several molecular mechanisms to ensure equal gene expression from the sex chromosomes between the sexes [2]. This process is known as dosage compensation. In *C. elegans,* hermaphrodites have two X chromosomes (2X:2A), whereas males have only one X and no other sex chromosome (1X:2A) [3]. This difference in chromosome count is essential for sex determination [3,4]. However, without correction, in hermaphrodites, transcription from the X doubles relative to males, leaving the hermaphrodite population inviable [5]. The dosage compensation mechanism in *C. elegans* corrects for the differing numbers of sex chromosomes by reducing the gene expression of the hermaphrodite X chromosomes [6]. Dosage compensation requires orchestrating several gene-regulatory events across X chromosomes in hermaphrodites to decrease gene expression by half.

A core component of the dosage compensation machinery in *C. elegans* involves a specialized condensin complex. Condensins are highly conserved protein complexes used in most cellular life, from prokaryotes to metazoans [7]. Condensin complexes are characterized by their ring-shaped structure, and they hydrolyze ATP to extrude DNA strands through the ring, thus leading to DNA coiling and loop formation [8]. This loop extrusion activity is thought to be essential for chromosome compaction in mitosis and meiosis [9]. Multicellular eukaryotes have two condensin complexes, condensin I and II, functioning in mitosis and meiosis [10]. Similarly, *C. elegans* utilizes condensin I and II complexes for chromosome compaction and segregation [11]. However, *C. elegans* has a third condensin complex that specifically functions in dosage compensation of the X chromosomes of hermaphrodites. The hermaphrodite-specific condensin is known as condensin I^{DC} (Dosage Compensation) [11,12]. Condensins are composed of two structural maintenance of chromosomes (SMC) proteins and three chromosome-associated polypeptides (CAP) [13,14]. Condensin I^{DC} earns its name due to the four shared protein subunits with condensin I. These subunits include the structural maintenance of chromosomes (SMC) protein MIX-1 and the chromosome-associated polypeptides (CAPs) CAPG-1, DPY-26, and DPY-28. The difference between condensin I^{DC} and condensin I is the second SMC subunit, DPY-27 in condensin I^{DC} and its paralog SMC-4 in condensin I [11,15,16]. Condensin I^{DC} compacts the dosage compensated X chromosomes; thus, the X occupies less nuclear volume in

hermaphrodites than in males [17,18]. At a higher resolution, condensin I^{DC} remodels the architecture of the X chromosomes to form topologically associating domains (TADs) characterized by a higher frequency of *cis*-interactions within domains [19,20].

Beyond condensin I^{DC}, the complete dosage compensation complex (DCC) in *C. elegans* includes the proteins SDC-1, SDC-2, SDC-3, DPY-30, and DPY-21 [11,21–23]. Together, these ten proteins bind and spread across the X chromosomes in hermaphrodites, inhibiting RNA Pol II binding, thus lowering transcriptional output by half [24]. One of the non-condensin DCC subunits is DPY-21 [22]. It contains a Jumonji C domain found in histone demethylases. DPY-21 has been shown to demethylate dimethylated histone 4 lysine 20 (H4K20me2) [25], previously deposited on histones by the activities of SET-1 and SET-4 [26,27], to the monomethylated form (H4K20me1). Thus, by the X-specific demethylase activity of DPY-21, H4K20me1 is enriched on the X chromosomes in hermaphrodites and contributes to further repression [25–27]. In addition to its demethylase function, DPY-21 has an additional uncharacterized role in dosage compensation [25,28]. Like other DCC members, DPY-21 activity is required to regulate the X chromosome effectively, as evidenced by the elevated X-linked gene expression in hermaphrodites with *dpy-21* mutations [25,29]. However, DPY-21 is not necessary to recruit the other DCC members, and the loss of its function leads to mild defects in hermaphrodite *C. elegans* but no significant lethality [22].

Nuclear lamina interactions with heterochromatin provide an additional layer of gene regulation in *C. elegans,* impacting dosage compensation. In *C. elegans,* heterochromatic regions of chromosomes are located near the nuclear periphery [29,30]. Histone methyl transferases (HMTs) MET-2 and SET-25 target H3 lysine 9 (H3K9) on chromatin to deposit mono-, di-, and trimethylation [30]. The lamina-associated protein CEC-4 binds to heterochromatic H3K9me regions on both the autosomes and the X [32]. The tethering of heterochromatic regions of the chromosomes to the nuclear lamina contributes to stabilizing cell fates during *C. elegans* development [32]. In addition, the loss of nuclear lamina tethering leads to the decompaction and relocation of the X into a more interior position in the nucleus and a mild increase of X-linked gene expression without impacting autosomal gene expression, indicating dosage compensation defects [33]. Despite defects in the chromosomal organization, mutants with non-functional CEC-4 survive with no apparent phenotypes [32].

Dosage compensation is set up in a stepwise manner over the course of development in *C. elegans*. The process is initiated around the 40-cell stage, when the DCC subunit SDC-2 is expressed and localizes to hermaphrodite X chromosomes [34], which leads to the recruitment of the other DCC subunits [35]. This initiation step coincides with the loss of pluripotency of embryonic blastomeres [36,37]. DPY-21 localizes to the X after the initial loading of condensin I^{DC}, and H4K20me1 becomes enriched on the X between the bean and comma stages of embryogenesis [25,36]. By the end of embryogenesis, most cells exit mitosis [38], after which the dosage-compensated state is maintained in

postmitotic cells. We refer to this stage as the maintenance phase. Earlier studies using cold-sensitive *dpy-27* alleles suggested that DPY-27 activity is essential during a critical developmental time window in mid-embryogenesis, after which loss of its function has a lesser impact on viability [39]. These results suggest that while condensin I^{DC} is required to initiate dosage compensation, other mechanisms may be responsible for maintaining repression once established, including ones mediated by DPY-21 and CEC-4.

The requirement for CEC-4 also changes with the differentiation state of embryonic cells. CEC-4 is required to tether heterochromatic transgenic arrays to the nuclear lamina in embryos but not in L1 larvae [32]. At the larval stages and beyond, additional mechanisms, including ones mediated by MRG-1 and CBP-1, contribute to sequestering heterochromatin to the nuclear lamina [40]. However, X chromosome compaction and nuclear lamina tethering are affected in *cec-4* adults, even in fully differentiated postmitotic cells [33]. We hypothesize that by sequestering the chromosome to the nuclear lamina, CEC-4 stabilizes the repression of the X chromosomes during the maintenance phase of dosage compensation.

In this study, we used the auxin-inducible degradation (AID) system to deplete the condensin I^{DC} subunit DPY-27 at various stages of development. We assessed the importance of condensin I^{DC} to X chromosome repression and organismal viability during the establishment and maintenance phases of dosage compensation. Our findings reveal that the continued presence of DPY-27 is required to maintain X chromosome repression after initial establishment. However, continued repression is less essential for viability during the maintenance phase. Additionally, we evaluated the hypothesis that the nuclear lamina protein CEC-4 helps stabilize the repressed state by combining *cec-4* mutations with depletion of DPY-27 or mutations in the histone demethylase *dpy-21.* We show that the loss of lamina associations resulting from mutations in *cec-4* exacerbates the defects caused by the lack of DPY-27 or DPY-21 function. Our results reveal the differential contributions of the various repressive pathways to X chromosome dosage compensation.

Results

The impact of DPY-27 depletion on hermaphrodite embryos and larvae

Using a strain containing an auxin-inducible degron (AID)-tagged *dpy-27* allele [41] and expressing the plant F-box protein TIR1 under a ubiquitous promoter (*eft-3*) [42] (referred to as *TIR1; dpy-27::AID*, for complete genotype and allele information for all strains see the Materials and Methods), we were able to time the depletion of DPY-27 by moving worms to auxin-containing plates during or after embryogenesis. To evaluate whether the lack of CEC-4 exacerbates the defects, we also generated a strain containing the *cec-4 (ok3124)* mutation in addition to *TIR1* and *dpy-27::AID* (referred to as *TIR1; dpy-27::AID; cec-4).* For controls, we used wild-type worms (N2), *cec-4* mutants, and a strain with AID-tagged *dpy-27* but no TIR1 expressing transgene (referred to as *dpy-27::AID).*

Our first experiment investigated the ability of embryos exposed to auxin to survive in the absence of DPY-27 throughout the entirety of embryonic development. To ensure that the maternally loaded DPY-27 is also depleted, we initiated our assay at the L4 larval stage of the parent before oocyte production begins **(Fig 1A)** [15]. L4 larvae were placed on auxin-containing plates for a 24-hour egg-laying period, after which the parents were removed. This procedure ensures that both *in-utero* and *ex-utero* development occurs in the presence of auxin. Strains not exposed to auxin were mostly viable, although the *dpy-27::AID*-containing strains had a very low, but statistically significant, level of lethality (**Fig 1B**, Fisher's exact test, p values listed in **S1 File**). While auxin treatment did not significantly impact the survival of control embryos (N2, *cec-4, dpy-27::AID),* 100% of *TIR1; dpy-27::AID and TIR1; dpy-27::AID; cec-4* worms died as embryos or L1 larvae **(Fig 1B)**. These results indicate that DPY-27 function during embryonic development is essential for the survival of hermaphrodite worms, which is consistent with previous studies [39].

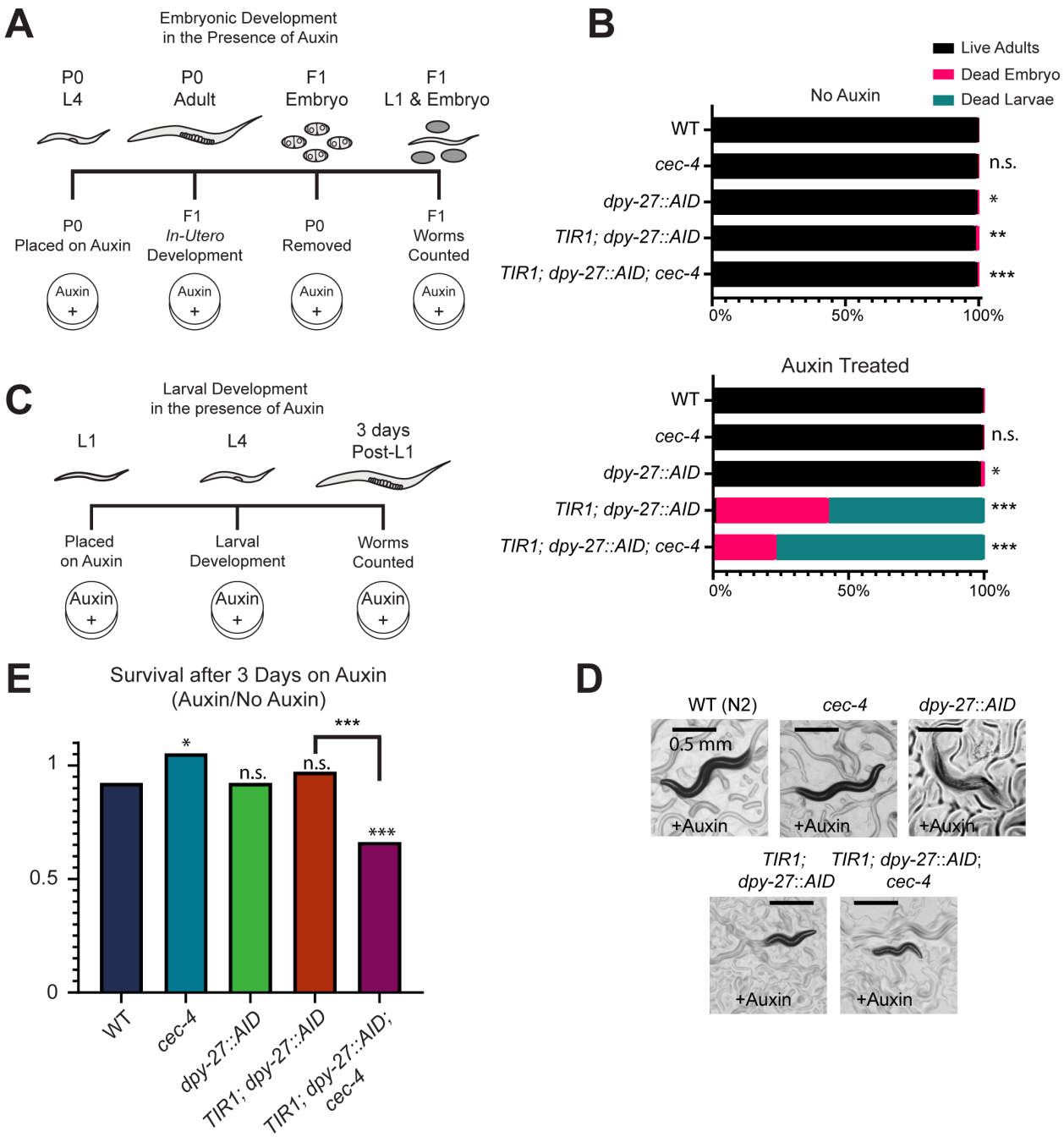

Fig 1. DPY-27 depletion leads to lethality and developmental defects. (A) Overview of the timeline of auxin exposure initiated from parental age L4 through F1 development. **(B)** Auxin exposure throughout embryogenesis results in compromised viability in *TIR1; dpy-27::AID* and *TIR1; dpy-27::AID; cec-4* strains. Total counts from three independent replicates are shown. N>600.Significance was determined by Fisher's exact test relative to wild-type values. Dead embryos and dead larvae were summed as one value for statistical analyses. Complete statistical analysis can be found in **S1 File**. **(C)** Overview of the timeline of auxin exposure from the L1 stage for three days. N2 worms in this time frame grow to young adults. **(D)** Phenotypic images of hermaphrodites exposed to auxin from the L1 stage for three days. Scale bar, 0.5 mm. **(E)** Larval survival on auxin relative to survival off auxin. Total counts from three

independent experiments are shown. N>600. Statistical significance was determined by Chi square tests. Complete statistical analyses can be found in **S2 File**. n.s. = not significant, * = $p < 0.05$, ** = $p<0.01$, *** = $p < 0.001$.

At the onset of dosage compensation during early embryogenesis, condensin I^{DC} loads onto the X chromosomes in hermaphrodites [15]. However, it is unclear whether the sustained presence of the complex is essential once dosage compensation is established. To assess the requirement for DPY-27 to remain on the X during larval development, we exposed our strains to auxin starting at the L1 larval stage for a period of three days. We compared survival on auxin-containing plates to survival on plates without auxin **(Fig 1C)**. Strains developing without auxin exposure grew to adulthood and produced viable offspring in the timeframe of the experiment. In contrast to embryonic exposure, exposing larvae to auxin had a much lesser effect on survival. Most *TIR1; dpy-27::AID* larvae survived similarly to N2, *cec-4*, or *dpy-27::AID* controls **(Fig 1E,** Chi-square test, p values listed in **S2 File)**. However, DPY-27 depleted strains developed slowly and exhibited developmental defects, including stunted growth **(Fig 1D)**. The rare embryo produced by these hermaphrodites did not hatch. Adding *cec-4* to the background lowered the survival rate, suggesting that lack of both DPY-27 and CEC-4 results in more severe defects than lack of DPY-27 alone **(Fig 1E)**.

Exposure to auxin rapidly depletes DPY-27

We next investigated the degree of DPY-27 depletion in auxin-treated strains relative to untreated. DPY-27 was visualized in each strain by immunofluorescence (IF) after worms were exposed to auxin for three days starting at the L1 larval stage. Due to the underdeveloped nature of the DPY-27 depleted strains, we based the timing of IF staining on the growth of wild type. After 3 days, wild-type N2 worms have developed into young adults. IF images were captured in intestinal nuclei. Intestinal cells are 32-ploid and their large size facilitates analyses of the nucleus. Before auxin treatment, all our strains had a wild-type pattern of DPY-27 localization within the nucleus of intestinal cells **(Fig 2A)**, consistent with the lack of any visible defects or lethality in these strains. Auxin treatment in N2, *cec-4*, and *dpy-27::AID* strains led to no observable changes. However, in the *TIR1*-containing strains, *TIR1; dpy-27::AID* and *TIR1; dpy-27::AID; cec-4,* auxin treatment resulted in depletion of DPY-27 to background levels **(Fig 2A)**, suggesting that auxin-induced degradation was successful.

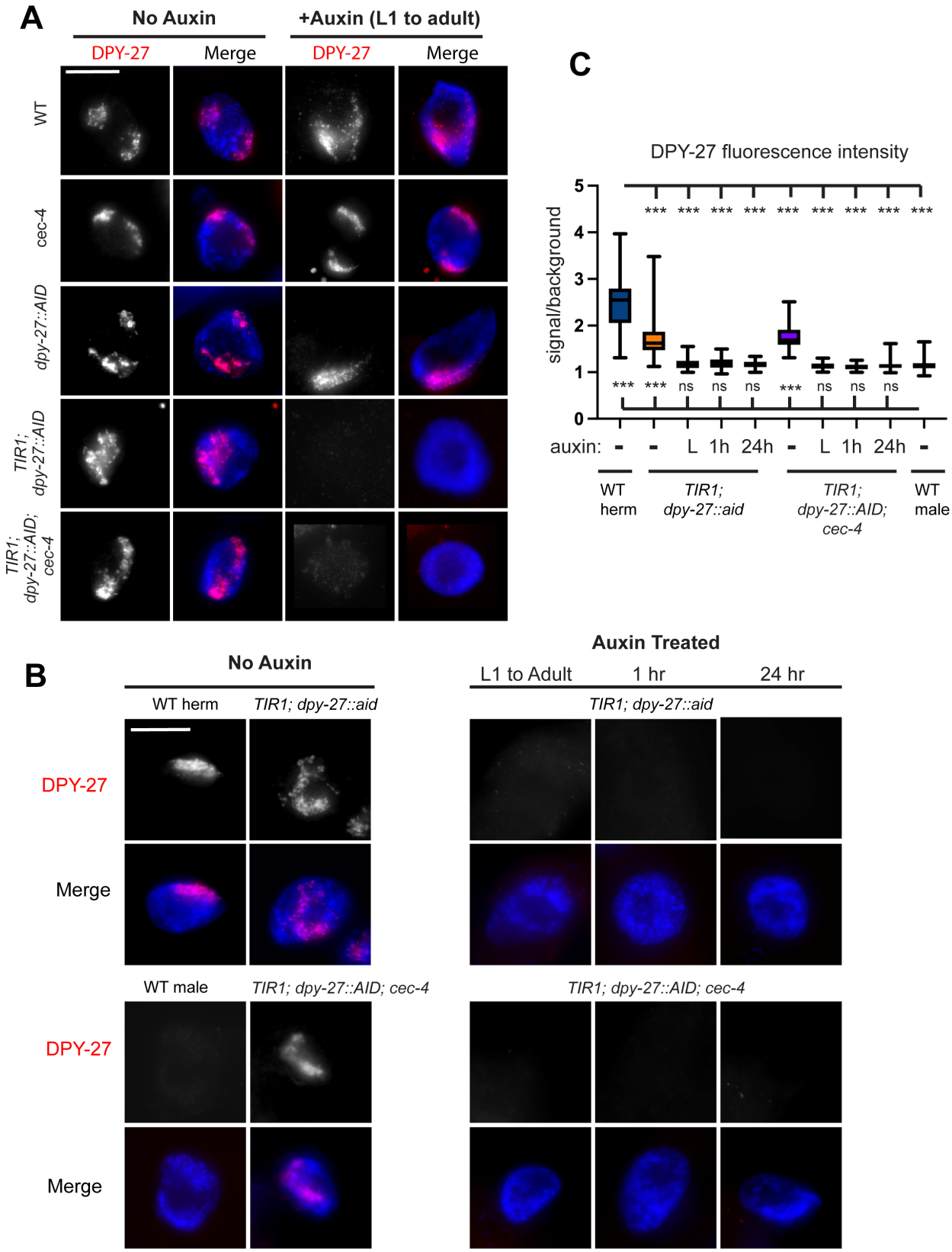
A
No Auxin
+Auxin (L1 to adult)
DPY-27
Merge
DPY-27
Merge
WT
cec-4
dpy-27::AID
TIR1; dpy-27::AID
TIR1; dpy-27::AID; cec-4
C
DPY-27 fluorescence intensity
signal/background
auxin: - - L 1h 24h - L 1h 24h -
WT herm
TIR1; dpy-27::aid
TIR1; dpy-27::AID; cec-4
WT male
B
No Auxin
Auxin Treated
L1 to Adult
1 hr
24 hr
WT herm
TIR1; dpy-27::aid
TIR1; dpy-27::aid
DPY-27
Merge
WT male
TIR1; dpy-27::AID; cec-4
TIR1; dpy-27::AID; cec-4
DPY-27
Merge

245

Fig 2. Auxin treatment leads to depletion of DPY-27. (A) Immunofluorescence staining of DPY-27 within the intestinal nuclei of young adult hermaphrodites. DAPI staining of DNA (blue) merged with DPY-27 signal (red) is also shown. DPY-27 is present within the nuclei in strains not exposed to auxin, but exposure to auxin for 3 days starting at L1 results in a significant depletion of DPY-27 signal in strains that contain *TIR1* and *dpy-27::AID.* Original unaltered images are shown on Fig S1. **(B)** DPY-27 staining after auxin exposure for various lengths of times (L1 to adult, 1 hour, or 24 hours). Images were acquired with identical exposure times. Original unaltered images, with HTZ-1 costain, are shown on Fig S1. Scale bars, 10 μm. **(C)** Quantification of DPY-27 fluorescence signal in experiments shown in (B). Quantification is based on measuring DPY-27 fluorescence in the nucleus, normalized to background level fluorescence, from between 38 and 50 nuclei total collected in three independent experiments. Worms were not exposed to auxin (-), exposed to auxin from L1 stage for three days (L), or exposed to auxin from day 1 of adulthood for 1h or 24 hours. Whiskers indicate min-max values. Statistical analysis was done using Brown-Forsythe and Welch ANOVA tests with multiple comparisons. Comparisons to WT hermaphrodites are shown above and comparisons to WT males are shown below the box plots. For p values and all pairwise comparisons see **S3 File**. n.s. = not significant, * = $p < 0.05$, ** = $p<0.01$, *** = $p < 0.001$.

To quantify the level of depletion and to test reproducibility, we performed three independent experiments and imaged nuclei from each using standardized exposure times to allow direct comparisons between samples (**Fig 2B** and **C**). We included WT males in the analysis. WT males do not express DPY-27 [15], and the level of DPY-27 fluorescence measured in males was interpreted as background. Anti-HTZ-1 (a histone H2A variant) staining was used as control (Fig S1). Variability between replicates is shown Figs S2 and S3. Quantification of nuclear DPY-27 fluorescence intensity over background fluorescence intensity showed that *TIR1; dpy-27::AID* and *TIR1; dpy-27::AID; cec-4* before auxin treatment had somewhat lower DPY-27 staining compared to WT, but significantly more than in males (**Fig 2C**). The somewhat reduced DPY-27 staining is consistent with a low level of lethality in these strains, and indicate that dosage compensation maybe slightly reduced compared to WT. In*TIR1; dpy-27::AID* and *TIR1; dpy-27::AID; cec-4* worms treated with auxin from L1 stage for three days, DPY-27 staining was indistinguishable from staining in WT males.

In the L1 to adult timeframe, intestinal nuclei undergo 4 rounds of endoreduplication and reach the stage of 32-ploidy [43]. To analyze the continued need for DPY-27 after these altered cell cycles have taken place and the cells have fully differentiated, we performed experiments where the auxin treatment began in adulthood (3 days past L1). These experiments also allowed to test the rapidity of auxin induced depletion of DPY-27. In previous studies in *C. elegans,* protein degradation was observable within 30 minutes [42]. We subjected adult hermaphrodites to auxin for one hour and for 24 hours. In *TIR1; dpy-27::AID* and *TIR1; dpy-27::AID; cec-4* strains, both treatments led to DPY-27 levels indistinguishable from what is seen in males **(Fig 2B,C)**, suggesting that one hour is sufficient to deplete DPY-27 protein levels to background. Independent repetitions of these experiments showed that rapid depletion of the protein is reproducible (**Fig S2** and **S3**).

290 ## DPY-27 depletion disrupts DCC binding and stability

291 To assess the binding of other condensin I^{DC} subunits to the X chromosome following
292 DPY-27 depletion, we performed IF staining for the subunit CAPG-1 [11]. In WT and
293 *cec-4* strains, CAPG-1 maintains a signal pattern indicative of X chromosome binding
294 both with and without auxin treatment (**Fig 3A**). However, in *TIR1; dpy-27::AID* and
295 *TIR1; dpy-27::AID; cec-4* after auxin treatment from the L1 stage for three days, the
296 CAPG-1 signal becomes non-specific and diffuse throughout the entire nucleus **(Fig**
297 **3A)**. Our results indicate that after prolonged auxin exposure, condensin I^{DC} no longer
298 maintains localization to the X chromosomes following DPY-27 depletion.

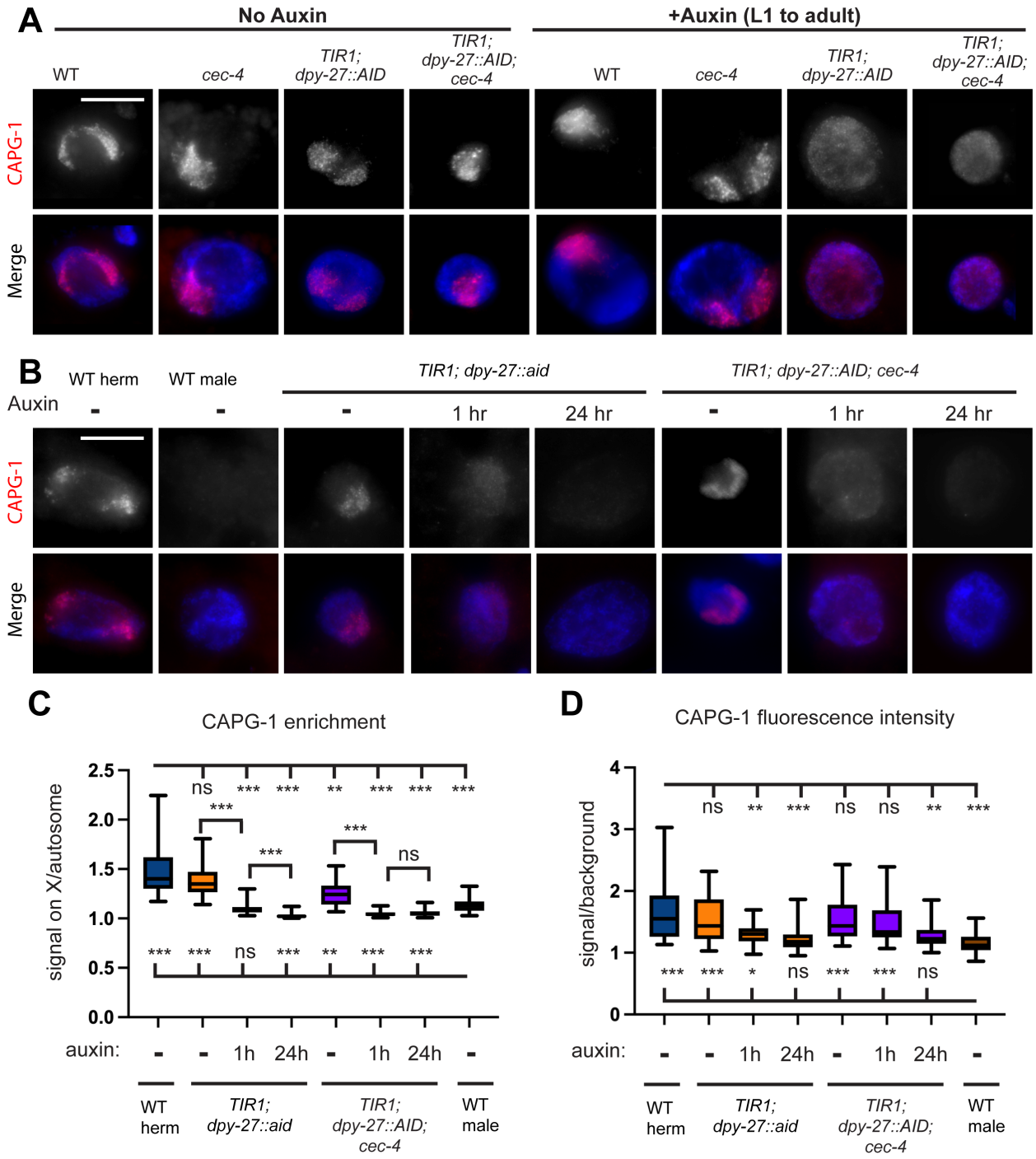

Fig 3. In the absence of DPY-27, condensin I^{DC} subunits become unstable. (A) Immunofluorescence staining of CAPG-1 within the intestinal nuclei of young adult hermaphrodites. DAPI staining of DNA (blue) merged with CAPG-1 signal (red) is also shown. DPY-27 is present within the nuclei in strains not exposed to auxin, but exposure to auxin for 3 days starting at L1 leads to lack of X enrichment of CAPG-1 signal in strains that contain *TIR1* and *dpy-27::AID.* Original unaltered images are shown on Fig S4. **(B)** CAPG-1 staining after exposing young adults to auxin for 1 hour or 24 hours. Images were acquired with identical exposure times. Original unaltered images (with HTZ-1 staining control) are shown on Fig S4.

308 Scale bars, 10 μm. **(C)** Quantification of CAPG-1 fluorescence signal in the enriched region over
309 non-enriched regions of the nucleus. Quantification is based on line-intensity scan analysis of
310 30-33 nuclei total collected in three independent experiments. Whiskers indicate min-max
311 values. Statistical analysis was done using Brown-Forsythe and Welch ANOVA tests with
312 multiple comparisons. Comparisons to WT hermaphrodites are shown above and comparisons
313 to WT males are shown below the box plots. For p values and all pairwise comparisons see **S4**
314 **File**. (**D**) Quantification of CAPG-1 fluorescence intensity in the nucleus, normalized to
315 background level fluorescence, from the same nuclei as in (C). Statistical analysis was done
316 using Brown-Forsythe and Welch ANOVA tests with multiple comparisons. Comparisons to WT
317 hermaphrodites are shown above and comparisons to WT males are shown below the box
318 plots. For p values and all pairwise comparisons see **S4 File**. n.s. = not significant, * = $p < 0.05$,
319 ** = $p<0.01$, *** = $p < 0.001$.

320 To determine how fast CAPG-1 dissociates from the X and to determine whether the
321 protein diffuses throughout the nucleus or becomes unstable, we again performed auxin
322 treatment for 1 hour and 24 hours on adult worms and used standardized exposure
323 times to image nuclei to be able to compare signal intensities across samples (**Fig 3B**).
324 We first quantified the enrichment of CAPG-1 in a region of the nucleus, which we
325 interpret as the X chromosomes, where CAPG-1 is known to localize to in WT worms
326 [11]. We used line intensity scan quantification to determine the difference between
327 CAPG-1 signal intensity in the enriched region over non-enriched region (**Fig 3C**, see
328 methods). CAPG-1 is enrichment again was somewhat lower in *TIR1; dpy-27::AID* and
329 *TIR1; dpy-27::AID; cec-4* strains prior to auxin treatment, similar to the slightly reduced
330 DPY-27 staining in these strains. After 1 hour or 24 hours of auxin treatment,
331 enrichment becomes indistinguishable from (or lower than) what is seen in males. Since
332 the level of enrichment seen in males we interpreted as being due to background
333 staining by the antibody, we do not believe that the statistically significantly lower values
334 in the *TIR1; dpy-27::AID* and *TIR1; dpy-27::AID; cec-4* strains has biological
335 significance. These results suggests that within 1 hour of the initiation of DPY-27
336 depletion, CAPG-1 is no longer noticeably enriched on the X chromosomes.

337 We also quantified total CAPG-1 fluorescence in these nuclei. Nuclei from non-auxin
338 treated *TIR1; dpy-27::AID* and *TIR1; dpy-27::AID; cec-4* worms had CAPG-1 staining
339 similar to WT hermaphrodites. Signal intensity was only partially reduced (*TIR1; dpy-*
340 *27::AID*) or similar to WT hermaphrodites (*TIR1; dpy-27::AID; cec-4*) after 1 hour of
341 auxin treatment. However, after 24 hours of auxin treatment in both strains, the signal
342 became indistinguishable from the signal seen in males that lack condensin I^{DC}.
343 Together with the enrichment analysis, these results suggests that the CAPG-1 protein
344 persists somewhat longer than DPY-27 after auxin treatment, but the protein present is
345 unable to localize to the X chromosomes and eventually degrades.

346 H4K20me1 does not persist on the X chromosomes after 347 DPY-27 depletion

348 We next assessed the enrichment of the histone modification H4K20me1 on the X. In
349 wild-type N2 hermaphrodites, this histone modification is specifically enriched on

350 dosage-compensated X chromosomes [26,27], and this pattern was maintained in *cec-4*
351 and WT strains after auxin treatment. However, after exposure to auxin from the L1
352 stage for three days in *TIR1; dpy-27::AID* and *TIR1; dpy-27::AID; cec-4* strains,
353 H4K20me1 was no longer specifically enriched in a region within the nucleus,
354 resembling the pattern observed for CAPG-1 localization **(Fig 4A)**. H4K20me1 first
355 becomes enriched on dosage-compensated X chromosomes in mid-embryogenesis
356 [27,36], well before the L1 stage, when auxin treatment was initiated. We conclude that
357 the continued presence of DPY-27 and the DCC is required to maintain the enrichment
358 of this chromatin mark on the X chromosomes during larval development.

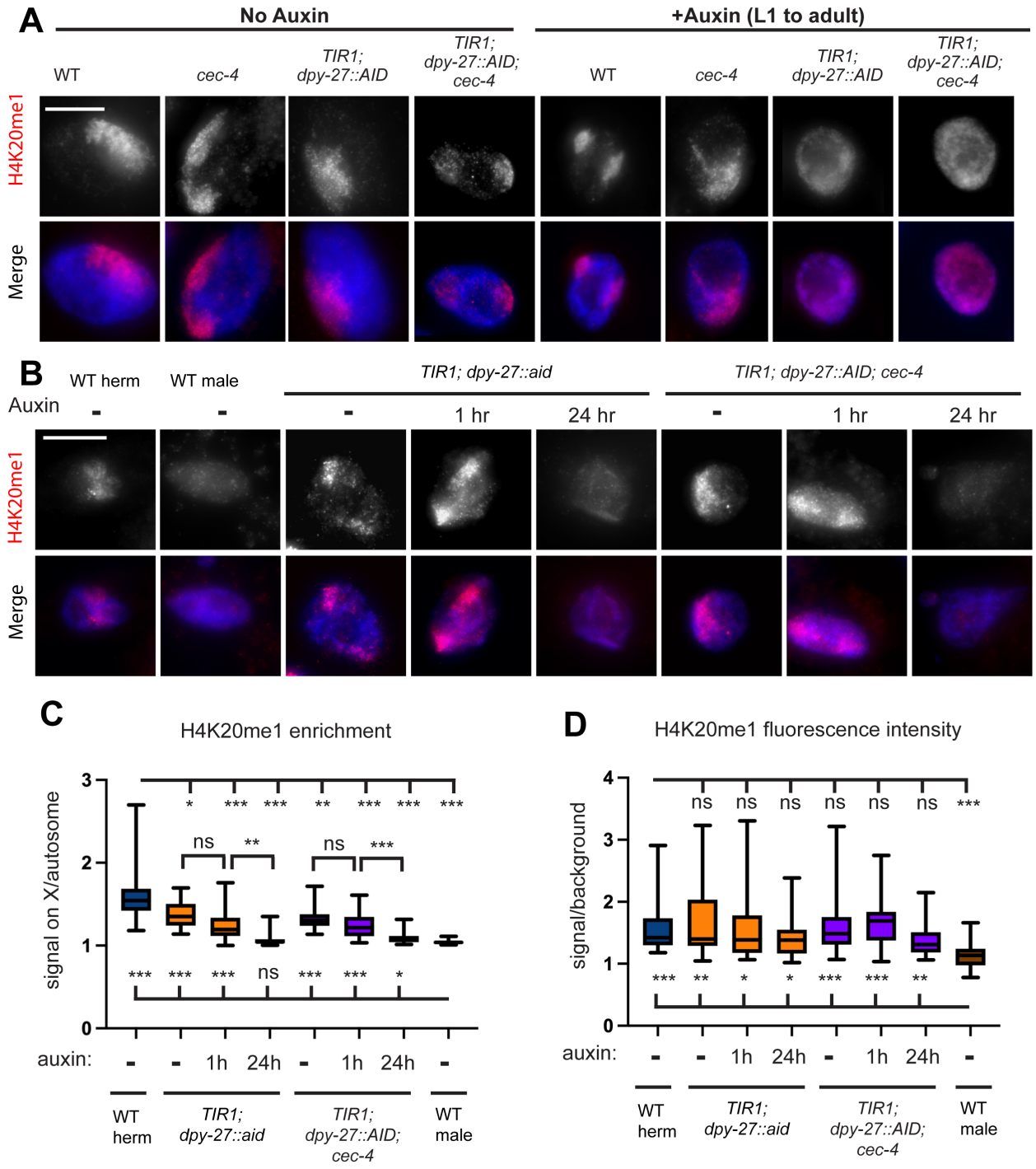

Fig 4. In the absence of DPY-27, H4K20me1 enrichment is lost. (A) Immunofluorescence staining of H4K20me1 within the intestinal nuclei of young adult hermaphrodites. DAPI staining of DNA (blue) merged with H4K20me1 signal (red) is also shown. H4K20me1 is clearly enriched in a region within nuclei (assumed to be the X) in strains not exposed to auxin. Auxin exposure for 3 days starting at L1 led to lack of X enrichment of H4K20me1 signal in strains that contain *TIR1* and *dpy-27::AID.* Original unaltered images are shown on Fig S5. **(B)** H4K20me1 staining after auxin exposure for 1hr or 24 hours. Images were acquired with identical exposure times. Original unaltered images (with HTZ-1 staining control) are shown on Fig S5. Scale bars, 10

368 µm. **(C)** Quantification of H4K20me1 fluorescence signal in the enriched region over non-
369 enriched regions. Quantification is based on line-intensity scan analysis of 29-30 nuclei total
370 collected in three independent experiments. Whiskers indicate min-max values. Statistical
371 analysis was done using Brown-Forsythe and Welch ANOVA tests with multiple comparisons.
372 Comparisons to WT hermaphrodites are shown above and comparisons to WT males are
373 shown below the box plots. For p values and all pairwise comparisons see **S5File**. (**D**)
374 Quantification of H4K20me1 fluorescence intensity in the nucleus, normalized to background
375 level fluorescence, from the same nuclei as in (C). Statistical analysis was done using Brown-
376 Forsythe and Welch ANOVA tests with multiple comparisons. Comparisons to WT
377 hermaphrodites are shown above and comparisons to WT males are shown below the box
378 plots. For p values and all pairwise comparisons see **S5 File**. n.s. = not significant, * = $p < 0.05$,
379 ** = $p<0.01$, *** = $p < 0.001$.

380 To assess how fast H4K20me1 enrichment is lost in postmitotic nuclei after DPY-27
381 depletion, we treated adult worms with auxin for 1 hour and 24 hours and quantified
382 enrichment and total fluorescence intensity of the H4K20me1 signal (**Fig 4B**). After 1
383 hour of auxin treatment, the signal remains clearly enriched in a portion of the nucleus
384 in both *TIR1; dpy-27::AID* and *TIR1; dpy-27::AID; cec-4* strains. However, after 24 hours
385 of auxin treatment, enrichment in both strains becomes similar to what is seen in males
386 (**Fig 4C**). Assessment of total H4K20me1 signal intensity (**Fig 4D**) was less conclusive
387 due to large cell-to-cell variation. Most genotypes had total fluorescence values not
388 statistically different from WT hermaphrodites. Overall, we can conclude that enrichment
389 of the H4K20me1 mark persists longer than the presence of condensin I^{DC} on the X, but
390 that enrichment does diminish within 24 hours. The *TIR1; dpy-27::AID* and *TIR1; dpy-*
391 *27::AID; cec-4* strains appeared similar in this assay (**S5 File**), suggesting that the
392 presence or absence of CEC-4 does not contribute to the maintenance of the
393 H4K20me1 mark.

394 The continued presence of DPY-27 is required to maintain X
395 chromosome condensation and subnuclear localization

396 The X chromosomes of wild-type hermaphrodites occupy a lower proportion of nuclear
397 space compared to what is predicted based on DNA content [17]. We previously
398 showed that in DCC mutants and in *cec-4* mutant hermaphrodites, the X chromosomes
399 decondense and relocate toward the more actively transcribed central region of the
400 nucleus [33]. The DCC starts to compact the X chromosomes in early embryogenesis
401 [17]. We tested if the continued presence of DPY-27 is necessary for maintaining the
402 compact conformation and peripheral localization of the X. We performed whole
403 chromosome X paint fluorescence *in situ* hybridization (FISH) to mark the X
404 chromosome territories in intestinal nuclei. Without auxin treatment, the X chromosome
405 signal appeared as expected: compact and near the nuclear periphery in all strains
406 without a *cec-4* mutation and more diffuse in strains with a *cec-4* mutation **(Fig 5A).**
407 After auxin treatment from L1 stage for 3 days, the X chromosomes appeared enlarged
408 in *TIR1; dpy-27::AID* as well. We quantified these changes by measuring the proportion
409 of nuclear volume occupied by the X chromosome (see Methods). The X chromosomes
410 occupied about 12-13% of the nuclear volume on average in wild type and close to 20%

411 in *cec-4* mutants **(Fig 5B)** which is consistent with previous results [33]. In the *TIR1;*
412 *dpy-27::AID* strain, depletion of DPY-27 led to decondensation of the X chromosome to
413 a degree similar to *cec-4* mutants or to what was previously observed in worms treated
414 with *dpy*-27 RNAi [17]. These findings demonstrate the critical role of DPY-27 in
415 maintaining the compact conformation of the X chromosome in wild-type
416 hermaphrodites. In the *TIR1; dpy-27::AID; cec-4* strain, the X was already decondensed
417 without auxin treatment due to the presence of the *cec-4* mutation, and depletion of
418 DPY-27 led to a measurable level of additional decondensation **(Fig 5B)**. These results
419 indicate that the presence of DPY-27 maintains X compaction, and the additional loss
420 off *cec-4* exacerbates the decondensation defects. To assess if shorter exposure to
421 auxin in postmitotic cells of adults is sufficient to lead to X decondensation, we
422 subjected young adult worms to 24 hours of auxin treatment. In both the *TIR1; dpy-*
423 *27::AID* and the *TIR1; dpy-27::AID; cec-4* strains, this treatment led to similar levels of
424 decondensation as seen after the longer L1 to adult exposure (**Fig 5B**). These results
425 indicate that the continued the presence of DPY-27 is required to maintain a compact X
426 structure even in fully differentiated postmitotic cells.

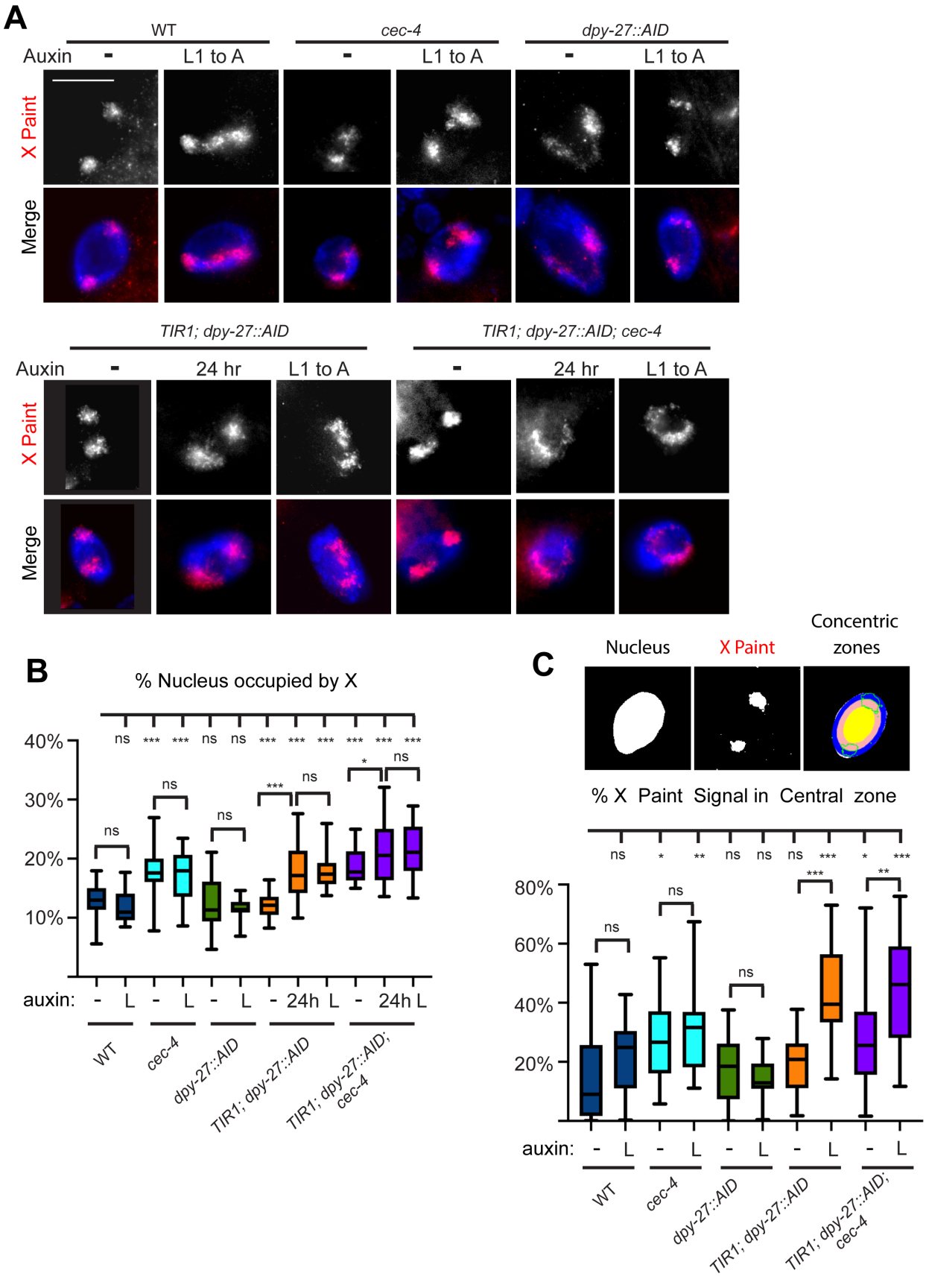
A
WT
cec-4
dpy-27::AID
Auxin
-
L1 to A
X Paint
Merge
TIR1; dpy-27::AID
TIR1; dpy-27::AID; cec-4
24 hr
B
% Nucleus occupied by X
40%
30%
20%
10%
auxin:
24h
WT
cec-4
dpy-27::AID
TIR1; dpy-27::AID
TIR1; dpy-27::AID; cec-4
C
Nucleus
X Paint
Concentric zones
% X Paint Signal in Central zone
80%
60%
40%
20%

427

Fig. 5. The continued presence of DPY-27 is required for X compaction and peripheral localization within the nucleus. (A) Intestinal nuclei from adult hermaphrodites were stained with whole X chromosome paint FISH probe (top row, red), and DNA was labeled with DAPI (blue). Images are of young adults not exposed to auxin, worms treated with auxin from L1 to adulthood, or young adults treated with auxin for 24 hours. Scale bars, 10 μm. Original unmodified images are shown on Fig S6. **(B)** Quantifications of the X chromosome volume normalized to nuclear size of worms grown auxin (-), worms treated with auxin from L1 stage for three days (L), and young adult worms treated with auxin for 24 hours (24h). **(C)** (top) Three-zone assay segmentation shown on a single slice from the middle of an intestinal nucleus. The amount of X signal (outlined in green) in each zone was quantified. (bottom) The proportion of the X paint signal seen in the central zone of the nucleus. In (C) and (D) 20-24 nuclei total from 3-4 independent experiments were quantified. Differences between samples were evaluated using unpaired Student's t-test. For complete statistical analysis see **S6 and S7 Files.** Analyses in all concentric rings can be found in **Fig S7.** n.s. = not significant, * = $p < 0.05$, ** = $p<0.01$, *** = $p < 0.001$.

Dosage compensation mechanisms make the X chromosomes not only compact but also position the chromosomes near the nuclear periphery [33]. To assess any changes in subnuclear localization, we analyzed our X chromosome FISH signals in the various strains using a three-zone assay (see Methods) **(Fig 5C).** The localization of the X within the nucleus was assessed in three concentric zones from a single focal plane taken from the middle of the nucleus, and the portion of the X signal in the central zone was quantified. In wild-type hermaphrodites, we observed the expected X localization. Only a small portion of the signal reaches into the central zone, while the bulk of the X is located in the intermediate and peripheral zones of the nucleus **(Fig 5C, Fig S7)** as observed before [33]. In *cec-4* mutants (*cec-4* and *TIR1; dpy-27::AID; cec-4)*, significantly more of the X signal is in the center, as expected. The relocation is even more significant in DPY-27 depleted strains **(Fig 5C)**. In both *TIR1; dpy-27::AID* and *TIR1; dpy-27::AID; cec-4* strains, over 40% of the signal is localized in the central zone, suggesting that the depletion of DPY-27 has a more significant impact on X nuclear localization than the *cec-4* mutation. We note that some of the apparent relocation could be a secondary consequence of decondensation. Adding a *cec-4* mutation did not significantly increase the degree of movement to the middle region compared to DPY-27 depletion alone (**S7 File**). Overall, these data indicate that the continued presence of DPY-27 is required to maintain the peripheral localization of dosage compensated X chromosomes.

DPY-27 is needed to maintain repression of X-linked genes

We next tested whether these changes in condensin I^{DC} localization, X chromosome compaction, nuclear organization, and the depletion of repressive histone marks, led to increases in X chromosome gene expression in the *TIR1; dpy-27::AID* and *TIR1; dpy-27::AID; cec-4* strains when treated with auxin. Although nuclear organization and H4K20me1 enrichment were not significantly different with and without a mutation in *cec-4*, the reduced viability of auxin-treated *TIR1; dpy-27::AID; cec-4* larvae compared to *TIR1; dpy-27::AID* larvae suggested that the X may be more derepressed in the strain also lacking *cec-4.* To test these hypotheses, we extracted total mRNA from

472 synchronized L3 populations, which were grown in the presence of auxin starting at L1
473 or grown in the absence of auxin for controls. We performed these experiments at the
474 L3 stage rather than at a later stage, because at this stage the delay in growth and
475 development of the DPY-27 depleted strains is not yet apparent, and also to avoid
476 complications arising from the contributions from the germline where the X
477 chromosomes are not subjected to dosage compensation [44]. At the L3 stage, the
478 germline consists of only about ~60 cells, and thus the RNA extracted from whole
479 worms represents predominantly somatic tissues [45]. Three replicates were analyzed
480 for each condition. PCA plots, hierarchical clustering, and Pearson correlation analyses
481 were used to evaluate data quality (Figs S8-S11). Since gene expression did not
482 change much in some samples compared to WT, these samples did not necessarily
483 cluster according to genotype. We therefore also performed analysis on a more limited
484 number of samples (Figs S8-S9).

485 To analyze X:A gene expression ratio, the mRNA-seq readout was plotted as a log2-fold
486 change in gene expression on autosomes and the X in auxin-treated samples compared
487 to controls **(Fig 6, Fig S12, S8 File).** Without exposure to auxin, the *dpy-27::AID* strain
488 had similar gene expression levels to N2, although the slight X derepression was
489 statistically significant. The minimal change in gene expression suggests that tagging
490 DPY-27 with the degron tag did not significantly disrupt its function **(Fig S12A)**. *cec-4*
491 strains treated with auxin also displayed slight X depression compared to *cec-4* mutants
492 without auxin exposure, indicating a minimal influence of auxin treatment on gene
493 expression regulation **(Fig S12B)**. The *TIR1; dpy-27::AID* and the *TIR1; dpy-27::AID;*
494 *cec-4* strains also had a small degree of X derepression compared to wild type even in
495 the absence of auxin, possibly due to somewhat leaky *TIR1* activity (**Fig S12C and D**),
496 which is a phenomenon noted by other research groups as well [46–48]. Therefore, to
497 assess the increase in X-linked gene expression resulting from the loss of DPY-27, we
498 compared gene expression levels in the same strain with and without auxin and/or in
499 auxin-treated strains with and without TIR1 expression **(Fig 6)**. In comparison to *dpy-*
500 *27::AID*, the strain *TIR1; dpy-27::AID* had significant upregulation of the X chromosome
501 when treated with auxin, while autosomal gene expression remained unchanged (X
502 derepression (defined as median X-linked log2 fold change – median autosomal log2
503 fold change) = 0.503) **(Fig 6A)**. Similarly, auxin-treated *TIR1; dpy-27::AID* exhibited
504 significant X derepression (0.435) compared to non-auxin-treated **(Fig 6B)**. These
505 results demonstrate that depletion of DPY-27 during the maintenance phase of dosage
506 compensation leads to a significant increase in X-linked gene expression.

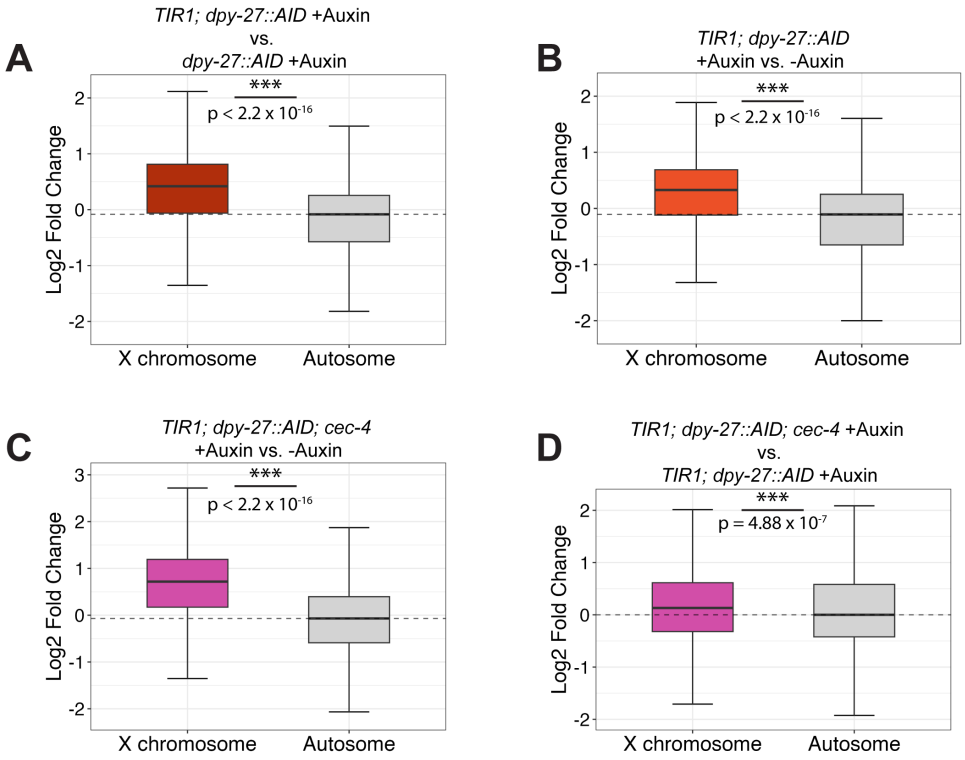

Fig 6. The X-linked genes are derepressed in strains depleted of DPY-27. (A-D) Boxplots depicting the distribution of the log2 fold change of X-linked genes and autosomal genes in strains being compared. A Wilcoxon rank-sum test was used to determine the statistical significance of the differential gene expression between the X and autosomes. (n.s. = not significant, * = p < 0.05, ** = p<0.01, *** = p < 0.001) **(A)** The log2 fold change in gene expression of the autosomes and the X chromosomes of *TIR1; dpy-27::AID* relative to the *dpy-27::AID* after both strains were exposed to auxin. **(B)***TIR1; dpy-27::AID* treated with auxin compared to the same genotype grown in the absence of auxin. **(C)** *TIR1; dpy-27::AID; cec-4* treated with auxin was compared to no auxin treatment. **(D)** *TIR1; dpy-27::AID; cec-4* compared to *TIR1; dpy-27::AID,* both treated with auxin. P values for all comparisons are listed in **S8 File**.

We then investigated whether the absence of CEC-4 further enhanced X derepression. Comparing the mRNA-seq gene expression profiles of *TIR1; dpy-27::AID; cec-4* treated with auxin to untreated populations of the same genotype, we observed a significant increase in X-linked gene expression (0.78) **(Fig 6C)**. The degree of X derepression was greater than that caused by auxin treatment in *TIR1; dpy-27::AID* without the *cec-4* mutation (X derepression of 0.435). These results suggest that the loss of *cec-4* may exacerbate X dosage compensation defects. To confirm, we compared *TIR1; dpy-27::AID; cec-4* to *TIR1; dpy-27::AID* after auxin treatment of both genotypes. The difference between these two populations was substantial (0.13), suggesting that depletion of DPY-27 leads to a greater level of X derepression in a strain that lacks CEC-4 **(Fig 6D)**. These results are consistent with CEC-4 playing a supporting role in helping to maintain stable X chromosome repression in differentiated cells.

531 To investigate the influence of *cec-4* in more detail, we used chromosome coordinates
532 of transcripts with changed gene expression to visualize the distribution of derepressed
533 regions in each comparison (**Fig S13**). CEC-4 binds to methylated H3K9 [32], a histone
534 modification which is enriched on the arms of autosomes and the left end of the X
535 chromosome [30]. These same genomic regions also make more frequent contacts with
536 nuclear lamina proteins [30][31]. We therefore considered the possibility that genes
537 whose expression changes due to the lack of *cec-4* would be preferentially located in
538 the left end domain of the X chromosome. Consistent with a general defect in dosage
539 compensation, in both the *TIR1; dpy-27::AID* and the *TIR1; dpy-27::AID; cec-4* auxin
540 treated strains compared to no auxin controls, we observed a general derepression
541 along the length of the X chromosomes (**Fig S13A** and **B**). Derepression was not more
542 evident along the left end of the chromosome in the *TIR1; dpy-27::AID; cec-4* strain (**Fig**
543 **S13B**), suggesting that the impact of the *cec-4* mutation does not preferentially effect
544 this chromosomal domain. When *cec-4* mutants were compared to WT, or when *TIR1;*
545 *dpy-27::AID; cec-4* on auxin was compared to *TIR1; dpy-27::AID* on auxin (**Fig S13C**
546 and **D**), similar conclusions were made. Gene expression differences were fairly evenly
547 distributed in the genome, with no apparent preferential impact along H3K9me enriched
548 domains. While somewhat surprising, these results are consistent with our previous
549 study in which we found that the CEC-4's effect on the X chromosome is more
550 chromosome-wide, and not limited to the left end domain [33] (see Discussion).

551 Loss of *cec-4* activity exacerbates dosage compensation
552 defects caused by a mutation in *dpy-21*

553 Our experiments showed that the loss of CEC-4 sensitizes hermaphrodite *C. elegans* to
554 dosage compensation defects caused by DPY-27 depletion **(Fig 6)**. To test whether
555 loss of CEC-4 also exacerbates defects caused by other dosage compensation
556 mutations, we sought to understand the interplay between CEC-4, known for its role in
557 tethering the X chromosomes to the nuclear lamina [33], and DPY-21, whose activity
558 leads to X-specific enrichment of H4K20me1 [25]. Individually, the mutations in these
559 pathways lead to phenotypes related to dosage compensation defects and changes in
560 X-linked gene expression, but despite these changes, the mutants are viable
561 [22,25,26,32,33]. Since *dpy-21* null mutants (*dpy-21(e428))* are viable [22], we
562 performed these experiments with the null mutant rather than using the AID system.
563 Therefore, our experiment tested the impact of these mutations throughout the lifespan
564 of the animals, including both the establishment and the maintenance phases of dosage
565 compensation. We constructed a double mutant *cec-4 (ok3124)* IV*; dpy-21(e428)* V
566 strain (referred to as *cec-4; dpy-21).* The strain is viable but with visible defects, such as
567 a Dpy phenotype.

568 We first evaluated the ability of hermaphrodites lacking functional *cec-4* and *dpy-21* to
569 lay viable eggs. The total number of eggs laid by *cec-4; dpy-21* hermaphrodites was
570 significantly smaller than all other strains observed, including the *dpy-21* and *cec-4*
571 single mutants **(Fig 7A)**. In all strains, most embryos hatched into larvae within 24

572 hours (**Fig 7B**). Most WT and *cec-4* mutant larvae developed into healthy adults. While
573 the viability of *dpy-21* mutant larvae was somewhat reduced, it was not significantly
574 different from the viability of *cec-4; dpy-21* double mutants **(Fig 7C).** Overall, these
575 results suggest that the addition of the *cec-4* mutation does decrease the overall fitness
576 of *dpy-21* mutants, most apparent in their ability to produce eggs.

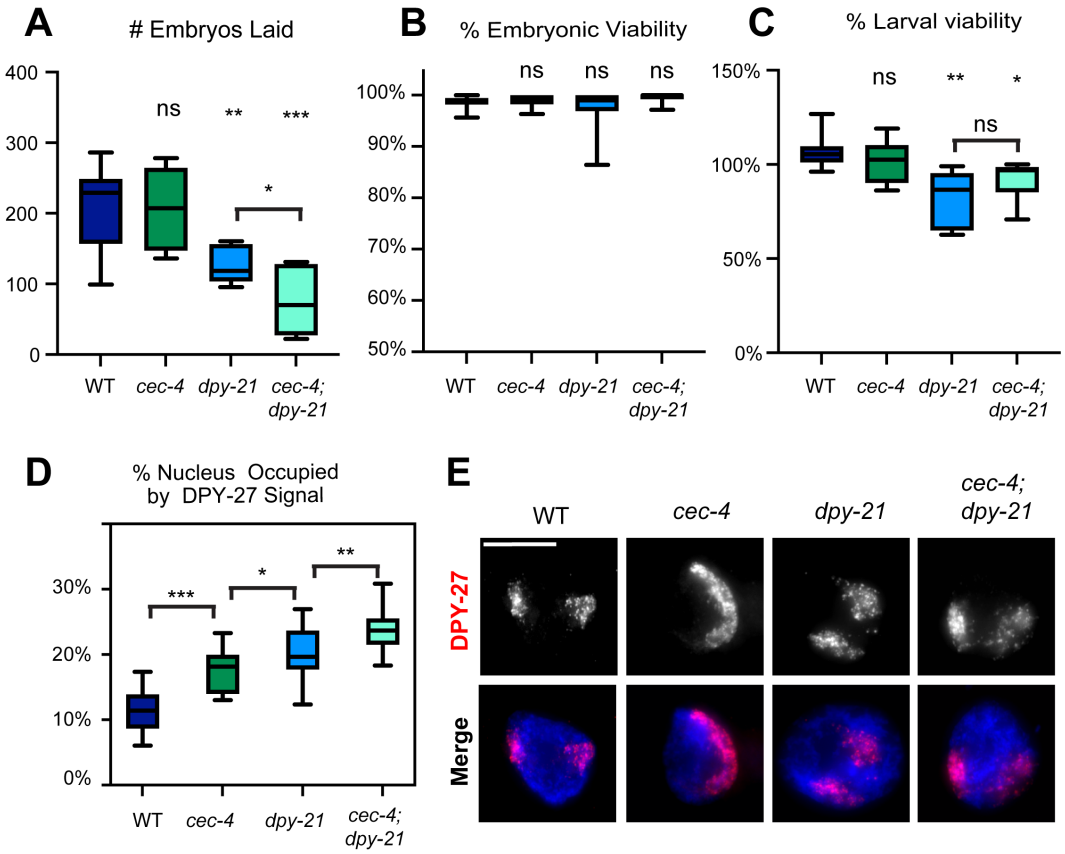

577

578 **Fig 7. Loss of CEC-4 exacerbates dosage phenotypes caused by mutations in *dpy-21*. (A)**
579 The average of total number of eggs laid per worm in WT, *cec-4, dpy-21,* and *cec-4; dpy-21*
580 backgrounds. **(B)** The average percentage of embryos that hatched after 24 hours. **(C)** The
581 average percentage of larvae that survived to adulthood. **(A-C)** Progeny from 6-8 individual
582 worms were scored per experiment for each genotype. Results shown are the combined
583 averages from three independent experiments (18<n<24). Statistical significance was
584 determined using Student's t-test. For statistical analysis and p values see S9 File. **(D)** The
585 extent of X chromosome decompaction in WT, *cec-4, dpy-21,* and *cec-4; dpy-21*
586 hermaphrodites. A total of 20 nuclei were analyzed from 3-5 independent experiments, no more
587 than 2 nuclei per individual worm. Statistical significance was determined using Student's t-test.
588 For statistical analysis and p values, see S10 File. **(E)** Representative images of adult
589 hermaphrodite intestinal nuclei stained for DPY-27 (top) and merged images of DPY-27 (red)
590 and DNA (DAPI, blue). Unmodified images are shown on Fig S14. Scale bar, 10 μm. n.s. = not
591 significant, * = p < 0.05, ** = p<0.01, *** = p < 0.001.

592 To assess the level of X chromosome compaction, we used DPY-27 IF to mark the
593 territories of the X chromosomes. DPY-27 maintains X localization in these mutants (**Fig**
594 **S15**), and previous studies have used DPY-27 staining in *cec-4* and *dpy-21* mutants to

595 analyze X chromosome compaction [25][49][50]. *cec-4* and *dpy-21* single mutants, as
596 well as the *cec-4; dpy21* double mutants all exhibited a prominently decondensed X
597 chromosome **(Fig 7E)**. Further quantitative analysis revealed that the X chromosomes
598 were decondensed in *cec-4* and *dpy-21* single mutants, but in the *cec-4; dpy-21* double
599 mutant strain the X occupied an even more significant proportion of the nucleus **(Fig 7D**
600 and **E)**. These observations show that adding the *cec-4* mutation to *dpy-21* mutants
601 augments some defects associated with dosage compensation.

602 To determine the impact of these mutations on X chromosome gene repression, mRNA-
603 seq was performed in L3 hermaphrodites **(Fig 8,** see **Figs S16 and S17** for correlation
604 and clustering analysis**,** and **S8 File** for statistical analysis**)**. We previously reported
605 subtle upregulation of the X chromosomes in *cec-4* mutant L1 larvae compared to the
606 wild type [33]. In L3 larvae, this upregulation was even more modest and not statistically
607 significant (X derepression = 0.027, p = 0.421) **(Fig 8A)**, suggesting that lack of CEC-4
608 alone does not have a significant impact on X-linked gene regulation despite the
609 observed changes in X chromosome compaction and nuclear localization. In contrast,
610 the *dpy-21* mutant displayed a more pronounced derepression of the X chromosome
611 (0.612, $p < 2.2 \times 10^{-16}$) **(Fig 8B)**, consistent with previous results [25,29]. When we
612 compared the *cec-4; dpy-21* double mutant to the wild type, we observed an even more
613 drastic change in gene expression (X depression = 0.721, $p = 2.2 \times 10^{-16}$) **(Fig 8C)**.
614 Furthermore, when juxtaposing the *cec-4; dpy-21* double mutant against its single
615 mutant counterparts, the results underscored that *cec-4; dpy-21* expressed X-linked
616 genes at a higher level than either single mutant (*cec-4; dpy-21* vs *cec-4* : X
617 derepression = 0.669, $p = 2.2 \times 10^{-16}$, and *cec-4; dpy-21* vs *dpy-21*: X derepression =
618 0.09, $p = 5.05 \times 10^{-13}$) **(Fig 8D** and **E)**. Given the relatively minor derepression of the X
619 chromosome in *cec-4* mutants, a significant increase in the X-linked gene expression
620 levels of *cec-4; dpy-21* compared to *cec-4* alone was expected **(Fig 8D)**. The *dpy-21*
621 single mutant already exhibited an upregulation in X chromosome gene expression;
622 however, the *cec-4; dpy-21* double mutant significantly surpassed it in X derepression
623 **(Fig 8E)**. While *cec-4*, as a single mutation, does not substantially impact X-linked gene
624 expression, our results show that the loss of *cec-4* sensitizes hermaphrodites to
625 additional dosage compensation defects.

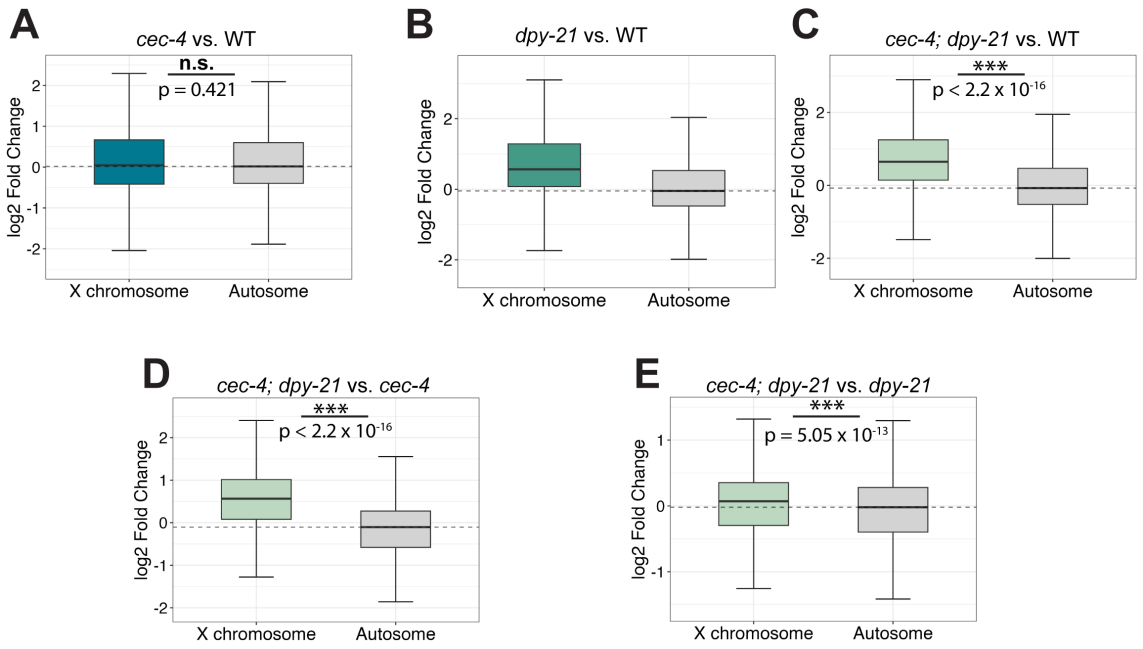

Fig 8. Loss of CEC-4 exacerbates gene expression defects caused by mutations in *dpy-21*. (A-E) Boxplots depicting the distribution of the expression change in X-linked genes and expression change in genes on autosomes is plotted as the log2 fold change of the strains being compared. Statistical significance is determined by the differences in gene expression between the X and autosomes by a Wilcoxon rank-sum test. (n.s. = not significant, * = $p < 0.05$, ** = $p<0.01$, *** = $p < 0.001$) **(A)** The log2 fold change in gene expression of the autosomes and the X chromosomes in *cec-4* mutant relative to the wild type (N2). **(B)** The log2 fold change in gene expression of the autosomes and the X chromosomes in *dpy-21* mutants relative to wild type (N2). **(C)** The log2 fold change in gene expression in *cec-4; dpy-21* relative to wild type (N2). **(D)** The log2 fold change in gene expression in *cec-4; dpy-21* compared to *cec-4*. **(E)** The log2 fold change in gene expression in *cec-4; dpy-21* compared to *dpy-21*. The derepression of the X chromosome genes is significantly higher in the double mutant than in single mutants.

Discussion

In this study, we investigated the relative importance of the DCC during two phases of dosage compensation: establishment and maintenance. We depleted DPY-27, a core protein subunit of the dosage compensation machinery, condensin I^{DC}, using the auxin-inducible degron system during embryonic and larval development. Our data indicated that DPY-27 function is essential during embryonic development, but the protein is dispensable for hermaphrodite survival during larval and adult stages. In an additional dosage compensation mechanism, the non-condensin DCC member DPY-21 significantly contributes to X-linked gene repression by enriching H4K20me1 on the X chromosome [25]. We show that the enrichment of H4K20me1 is lost rapidly after DPY-27 depletion, indicating that the mark must be continuously maintained, presumably by DPY-21 recruited to the X by DPY-27. In addition, DPY-27 depletion leads to X chromosome decondensation and relocation to a more central position in the nucleus, as well as significant increases in X-linked gene expression. In addition to the contributions of the DCC, nuclear lamina association of the X chromosome via

654 H3K9me3 binding to CEC-4 also contributes to X morphology and repression [33]. We
655 found that a loss-of-function mutation in *cec-4* amplifies the sensitivity of
656 hermaphrodites to the depletion/mutation of other dosage compensation processes.
657 These results suggest that nuclear lamina anchoring by CEC-4 serves to stabilize
658 repression initiated by condensin I^{DC} or H4K20me1. By loss-of-function mutations in
659 *cec-4* and *dpy-21* and depletion of DPY-27, we unexpectedly revealed that larval and
660 adult hermaphrodites are resilient to depletion of known dosage compensation
661 mechanisms and substantial increase in X-linked gene expression.

662 Condensin I^{DC} function is required for embryonic viability but not for 663 larval and adult viability

664 A previous study using a cold-sensitive mutant for *dpy-27* demonstrated that inactivating
665 DPY-27 during the comma stage of embryonic development leads to more extensive
666 lethality than inactivation of the protein at later stages. However, the differences in
667 viability counts at the different temperatures were only about 20% [39]. We re-examined
668 this question using the auxin-mediated degradation system, where adding auxin leads
669 to rapid and near complete depletion of DPY-27. Prior to auxin treatment, the strains
670 had essentially 100% viability, while auxin treatment during embryogenesis led to
671 essentially 100% lethality. These results demonstrate that condensin I^{DC} activity is
672 essential during embryonic development when cell fates are being specified, and cells
673 begin to differentiate into different cell types. At the end of embryonic development, the
674 embryo consists of about 500 cells, the majority of which have exited the cell cycle and
675 begun terminal differentiation [38]. Depletion of condensin I after embryogenesis is not
676 incompatible with viability despite developmental abnormalities in depleted larvae. This
677 result raised two possibilities. First, it is possible that dosage compensation, once
678 established, can be maintained in the absence of condensin I^{DC}. Second, it is possible
679 that X chromosome repression is not maintained but the larvae can tolerate defects in
680 X-linked gene regulation. Our results, discussed below, are consistent with the second
681 scenario.

682 Condensin I^{DC} must remain on the X to maintain the condensed 683 conformation

684 We show that compaction of the dosage compensated X cannot be maintained without
685 DPY-27. By varying durations of auxin exposure and observing the condensin I^{DC}
686 subunit CAPG-1, we saw the loss of condensin I^{DC} enrichment on the X and the gradual
687 loss of CAPG-1 signal from the nucleus **(Figs 2 and 3)**. We propose that the absence of
688 DPY-27 leads to the destabilization of the condensin I^{DC} ring, resulting in the release of
689 the complex from the X and gradual degradation of other complex members. The X
690 chromosome also decondenses after condensin I^{DC} loss, indicating that chromosome
691 compaction must be actively maintained. Previous research investigating the
692 maintenance of mitotic or meiotic chromosome architecture demonstrated that
693 depletion or inactivation of mitotic condensin subunits after chromosome condensation
694 has taken place leads to disorganized chromosome structure with reduced rigidity or a

larger surface area [51–54]. Similar to what we observed about the continued need for condensin I^{DC} to maintain the compact structure of dosage compensated X chromosomes, maintenance of mitotic chromosome architecture also requires the continued presence of condensin. However, in the studies of mitotic chromosomes, compaction was maintained after condensin loss, only the organization or rigidity of chromosomes was altered. In our study, compaction of the interphase X chromosome was not maintained. It has been suggested that during mitosis additional mechanisms, such as posttranslational histone modifications, contribute to chromosome condensation [55]. We hypothesize that in the absence of these mitosis-specific histone modifications in interphase, condensin function is necessary for compaction. We note that two posttranslational histone modifications associated with mitosis, namely enrichment of H4K20me1 and depletion of H4K16ac, are also features of interphase dosage compensated X chromosomes of *C. elegans* [26,27,55–57]. However, additional mitotic histone modifications that are not present on dosage compensated X chromosomes (for example H3S10Ph or depletion of additional acetylation marks) may also contribute to condensin independent chromosome compaction in mitosis [58]. Our findings indicate that the complete condensin complex must remain associated with the X for the maintenance of compaction during developmental stages in which most cells are post-mitotic. A recent study employed TEV protease-mediated cleavage of DPY-26, a subunit of condensin I^{DC} to inactive the complex. Cleavage of DPY-26 in the L1 stage led to loss of TAD structures from the X, suggesting that condensin I^{DC} is also required to maintain the fine-scale structural organization of the chromosome [59]. Compaction and organization of the chromosome into TADs are separable functions, as it is possible to disrupt TADs without loss of compaction [49]. Our results, together with the study by Das et al [59], suggest that the continued presence of condensin I^{DC} is required to maintain both levels of chromosomal organization.

In the absence of both condensin I^{DC} and CEC-4, the structure of dosage compensated X chromosomes is even more disrupted. However, the exact role of CEC-4 in the process remains unclear. We previously showed that the impact of CEC-4 on X chromosome compaction is most pronounced in the middle gene-rich domain, and the left arm the chromosome remains relatively unaffected [50]. Gene expression changes on the X were also not limited to the H3K9me3-enriched domain (to which CEC-4 binds) both in our previous study [50] and our current one (**Fig S13**). Thus, the effect appears more chromosome-wide. This is consistent with previous studies that showed a lack of correlation between DCC binding site on the X and genes being regulated by dosage compensation [60][61], and a lack of correlation between DCC-induced TAD formation and changes in gene expression [19]. Thus, it has been suggested that dosage compensation impacts gene expression more in a chromosome-wide manner, rather than locally by regulating individual genes.

The presence of DPY-27 is required to actively maintain the enrichment of H4K20me1 on the X

Shortly after the loss of DPY-27 signal, the H4K20me1 mark exhibits a loss of specific localization on the X with increasing auxin exposure time **(Figs 2 and 4)**. We propose that the continued presence of DPY-21 (presumable recruited by DPY-27) on the X is necessary to maintain H4K20me1 enrichment on the X. Notably, the presence of DPY-21 is not essential for the localization of condensin I^{DC} on the X; however, for DPY-21 to bind the X, the presence of condensin I^{DC} is required [22]. Our results are similar to what was seen for H3K9me2 and MET-2. Maintenance of this chromatin mark in *C. elegans* also requires the continued presence of the enzyme that places it [62]. Our results suggest that functional condensin I^{DC} plays a role in maintaining the localization of DPY-21 on the X, and its continued presence is required even in post-mitotic developmental stages. We hypothesize that in the absence of DPY-27 and DPY-21, either there is frequent enough histone turnover to lose the H4K20me1 enrichment or that the X is rendered accessible to histone modifiers that remove the H4K20me1 or modify the mark to di- or trimethylation.

Condensin I^{DC} is required to maintain X-linked gene repression in hermaphrodites

Severe depletion or mutation of dosage compensation in *C. elegans* is hermaphrodite lethal. Unexpectedly, we observed that hermaphrodites survive as larvae with near complete depletion of DPY-27, albeit with major phenotypic defects **(Fig 1C).** Furthermore**,** they survive without other vital contributors to X-linked gene regulation in addition to DPY-27 depletion, namely, nuclear lamina tethering by CEC-4 and H4K20me1 **(Fig 1 and 4)**. In short, auxin-treated *TIR1; dpy-27::aid; cec-4* larvae survive without measurable activity of any known dosage compensation mechanism. Our study revealed increases in X-linked gene expression beyond levels reported in *dpy-27* null mutant embryos or L1 larvae (log2 fold change in X-linked gene expression of less than 0.3) [29] or *sdc-2* mutant embryos treated with *sdc-2* RNAi (log2 fold change about 0.6) [49]. Dosage compensation defects in these mutants lead to lethality. Our most significant increase in X-linked gene expression was measured in *TIR1*; *dpy-27::AID; cec-4* L3 larvae after auxin exposure with a log2 fold change in X-linked gene expression at a value of 0.78 **(Fig 5)**. These larvae survive despite more significant gene expression defects than previously reported for embryos dying of dosage compensation defects. We suggest that the absence of these dosage compensation processes is acceptable in these animals because the continued repression of the X is no longer essential after early development once cell fates have been specified and the cells have differentiated.

In mice, the critical contributor to dosage compensation, the long non-coding RNA *Xist*, can be deleted with minimal change to X repression as long as it is deleted during the maintenance phase after X chromosome inactivation is fully established [63,64]. However, unlike the continued repression of the mouse X despite the loss of *Xist*, we

775 observed a significant derepression of X-linked genes in *C. elegans* hermaphrodites
776 after the depletion of DPY-27. Derepression was also observed in a recent study after
777 inactivation of condensin I/I^{DC} during the L1 stage [59]. The difference between dosage
778 compensation maintenance in mice and *C.* elegans might be due to the nature of the
779 repressive mechanisms. In mice, X chromosome inactivation involves the establishment
780 of facultative heterochromatin on the X chromosomes, including DNA methylation and
781 heterochromatic histone modifications [65]. Studies in other organisms have shown that
782 these chromatin marks can be maintained by propagating them during the S phase [66–
783 69], even without the initial trigger. The repressive mechanisms involved in *C. elegans*
784 dosage compensation are different. H4K20me1 patterns are not propagated during
785 DNA replication; in fact, H4K20me1 levels decrease in S phase due to the activity of an
786 H4K20me1 demethylase PHF8 [70]. Instead, H4K20me1 is thought to be established
787 during mitosis [56] and then converted to H4K20me2/3 methylation after mitotic exit
788 [56]. Our results suggest that maintenance of this mark on dosage compensated X
789 chromosomes requires the continued presence of DPY-27, presumably recruiting the
790 H4K20me2 demethylase DPY-21 [25].

791

792 The loss of function of cec-4 sensitizes hermaphrodites to the loss of 793 DPY-27 or DPY-21

794 The *cec-4* mutation, combined with DPY-27 depletion, showed only minor changes in
795 nuclear compartmentalization and chromosome compaction compared to DPY-27-
796 depleted strains with functional CEC-4 (**Fig 5)**. However, there was a notable decrease
797 in hermaphrodite viability of DPY-27 depleted larvae with a *cec-4* mutation compared
798 DPY-27 depleted larvae without a *cec-4* mutation (**Fig 1E**), suggesting disruption to X-
799 linked gene regulation approaching unacceptable limits for survival. When a *cec-4*
800 mutation was combined with a *dpy-21* mutation, there was an observable increase in X
801 decompaction and a decrease in brood size in the double mutant compared to single
802 mutants, again suggesting greater disruption to dosage compensation (**Fig 7**). mRNA-
803 seq analysis indicated that the loss-of-function mutation of *cec-4* alone minimally
804 increased X-linked gene expression **(Fig 8A)**. However, in scenarios where a *cec-4*
805 mutation was coupled with DPY-27 depletion or *dpy-21* mutation, we observed a
806 substantial increase in X-linked gene expression, significantly more than in strains
807 without the *cec-4* mutation **(Figs 6** and **8)**. Previous studies have highlighted the
808 involvement of CEC-4 in cellular differentiation and stabilizing cell fates [32]. Cells
809 actively undergoing differentiation demand precise gene expression levels. However,
810 we hypothesize that the loss of some repressive mechanisms after differentiation are
811 acceptable, partly because CEC-4 may help lock down established gene expression
812 patterns, including the repressed state of dosage-compensated X chromosomes. It
813 should be noted, however, that the loss of *cec-4* challenges the health of *C. elegans*
814 larvae depleted of other dosage compensation proteins, but most of the larvae survive.
815 We hypothesize that losing these mechanisms, including CEC-4 function, at the larval

developmental stage does not result in outright lethality because cellular differentiation is more complete.

While DCC-mediated mechanisms are crucial for viability during the establishment of dosage compensation, our results demonstrate that they are not essential for survival during the maintenance stage. During larval and adult developmental stages, hermaphrodites survive without any known dosage compensation activity. This resilience raises questions about the necessity of continued X repression after embryonic development.

Acknowledgments

We thank Sarah VanDiepenbos, Hend Almunaidi, and Lillian Tushman for their contributions to a preliminary analysis of the *cec-4 and dpy-21* mutants, as well as all members of the laboratory for helpful discussions. We would like to thank the laboratory of Dr. JoAnne Engebrecht for sharing the JEL1197 strain [41]. This work was supported by the National Institute of General Medical Sciences (https://www.nigms.nih.gov/), grants number R01 GM13385801 to GC, and R35GM149543 to GC and the National Science Foundation (https://www.nsf.gov/) grant number MCB 1923206 to GC. Some C. elegans strains used in this study were obtained from the Caenorhabditis Genetics Center (CGC), which is funded by the NIH Office of Research Infrastructure Program (P40 OD010440). The funders had no role in the study design, data collection and analysis, decision to publish, or preparation of the manuscript.

Materials and Methods

Caenorhabditis elegans Strains

The strains used are shown in the table below. Strains were maintained at 20°C on nematode growth media (NGM) plates seeded with the *Escherichia coli* strain OP50 as a food source, as described in [71]. For some experiments requiring larger number of worms, strains were grown on high-growth media (HGM) plates were seeded with *E. coli* strain NA22, as described in [72].

Genotype	**Strain**	**Source**
Wild Type	Bristol N2	CGC
dpy-21(e428) V	EKM71	This study
cec-4 (ok3124) IV	EKM121	This study
cec-4 (ok3124) IV; *dpy-21(e428)* V	EKM222	This study
ieSi57[Peft-3::*TIR1*::mRuby::unc-54 3'UTR, cb-unc-119(+)] II; *dpy-27*::*AID::MYC* (xoe41) III	EKM237	This study
dpy-27::AID::MYC (xoe41) III	EKM227	[41]

dpy-27::AID::MYC (xoe41) III; *cec-4* (ok3124) IV	EKM233	This study
ieSi57[Peft-3::*TIR1*::mRuby*::unc-54* 3'UTR, *cb-unc-119*(+)] II; *dpy-27::AID::MYC*(xoe41) III; *cec-4*(ok3124) IV	EKM238	This study
wrdSi3 [*sun-1*p::*TIR1*::F2A::mTagBFP2::AID*::NLS::tbb-2 3'UTR] II; *dpy-27*(*xoe4*1[*dpy-27::AID::myc*]) III; *him-8* (*me4*) IV	JEL1197	[41]
unc-119 (*ed3*); ieSi57 [*Peft-3*::*TIR1*::mRuby::*unc-54* 3'UTR, *cb-unc-119*(+)] II	CA1200	[42]

The alleles for *dpy-21 (e428)* and *cec-4 (ok3124)* were initially acquired from the *Caenorhabditis* Genetics Center (CGC) as the strains CB428 and RB2301, respectively. Each strain was backcrossed to Bristol N2 six times to generate the strains EKM71 *dpy-21 (e428)* and EKM121 *cec-4 (ok3124)*. EKM222 was obtained by crossing EKM71 to EKM121.

The strain JEL1197 was received from and generated by [41]. To isolate the *dpy-27::AID::MYC* (xoe41) allele, JEL1197 was crossed to wild type to produce EKM227. EKM227 was then crossed to CA1200 [42] to create EKM237.

To add *cec-4 (ok3124)* to the background, EKM227 was crossed with EKM121. The subsequent strain, EKM233, was crossed with CA1200 to generate EKM238.

Antibodies

Antibodies used in this study include rabbit anti-H4K20me1 (Abcam ab9051), rabbit anti-DPY-27 [11], rabbit and goat anti-CAPG-1 [33], and rat anti-HTZ-1 [73]. Secondary anti-goat, anti-rat, and anti-rabbit antibodies were purchased from Jackson Immunoresearch.

Synchronized worm growth and collection

To obtain synchronized worm populations, gravid adults were bleached to collect embryos [74]. During bleaching, the hermaphrodites degrade and leave only embryos, which are then collected. After washing with sterile 1X M9 salt solution [75], the embryos are isolated and shaken slowly overnight in a flask containing M9 buffer to allow them to hatch. Synchronized L1s were plated onto either NGM with OP-50 or HGM with NA22 plates as needed. Synchronized L1s were used in RNA-seq, IF, and larval development assays. After synchronization, L1s were grown to L3, or adult as needed per assay.

Auxin Treatment

Strains were subjected to auxin (Thermo Fisher Alfa Aesar Indol-3-Acetic Acid #A10556) by incorporation into NGM or HGM plates at a final concentration of 4mM, as

872 described in [42,76]. Auxin-containing plates were maintained in the dark at 4°C for up
873 to a month.

874 Assay of viability upon auxin exposure initiated during
875 embryogenesis

876 L4 hermaphrodites were placed on an auxin-containing plates or NGM plates for
877 controls to ensure all embryonic development occurs while exposed to auxin. Plates
878 were maintained in the dark at 20°C. Worms were placed on plates with or without auxin
879 for an egg-laying period of 24 hours. After this period, the adult was removed from the
880 plate, and the embryos laid were counted. 24 hours later, the number of dead larvae
881 and dead embryos were quantified. Live adults were counted 3 days after the initial egg-
882 laying period. Three independent replicates were performed. Differences were
883 evaluated using Fisher's exact test comparing the numbers of dead and live progeny for
884 each genotype.

885 Assay of viability upon auxin exposure initiated during larval
886 development

887 Experiments testing larval development began with synchronized L1 larvae. The
888 synchronized population was resuspended in M9 and split evenly between an auxin
889 plate and a plate without auxin for 3 days. Worms surviving after 3 days were counted.
890 Assuming an equal number of larvae initially plated, the final counts are reported as a
891 ratio of survival on auxin to survival off auxin. Three independent replicates were
892 performed. Differences were evaluated using Chi square test comparing the number of
893 surviving worms on auxin to the number surviving off auxin of each genotype.

894 Brood Count Assay

895 Young adult hermaphrodites were allowed to lay eggs on NGM and moved to new
896 plates each day until fertilized embryos were no longer produced. For each plate, after
897 removal of the parent, the number of embryos laid were counted, and after 24 hours,
898 the number of dead embryos were counted. After 3 days of development, the number of
899 surviving adults were counted. Embryonic viability was quantified as the number of
900 hatched embryos/total embryos. Larval viability was quantified as total number of
901 adults/hatched embryos.

902 Immunofluorescence (IF)

903 Hermaphrodite worms were dissected in 1x sperm salts (50 mM Pipes pH 7, 25 mM
904 KCl, 1 mM $MgSO_4$, 45 mM NaCl, and 2 mM $CaCl_2$) and fixed in 4% paraformaldehyde
905 (PFA) diluted in 1X sperm salts on a glass slide for 5 minutes in a humid chamber
906 containing PBS-T (PBS with 0.1% and Triton X-100). Slides were frozen on dry ice for
907 at least 20 minutes with a 20x20 mm coverslip over the diluted PFA and dissected *C.*
908 *elegans*. Using a razor blade, the coverslip was removed by flicking the coverslip off the
909 slide. The slides were then washed in PBS-T 3 times for 10 minutes each. 30µL of
910 diluted primary antibody was applied to each slide, a piece of parafilm was placed over
911 the spot with the antibody to slow evaporation. The slides were incubated in a humid

912 chamber at room temperature overnight. Slides were washed in PBS-T 3 times for 10
913 minutes and stained with corresponding secondary antibodies diluted 1:100 in PBS-T at
914 37°C for 1 hour. Three more washes in PBS-T were completed after the secondary
915 antibody incubation. In the third wash, the nucleus was stained using DAPI diluted in
916 PBS-T for 10 minutes at room temperature. Slides are mounted in Vectashield (Vector
917 Labs).

918 Fluorescence *in situ* Hybridization (FISH)

919 Degenerate Primer PCR was used to amplify purified yeast artificial chromosomes
920 (YACs) containing sequences corresponding to regions of the X chromosome and then
921 labeled with dCTP-Cy3 alongside standard nucleotides using random priming as in
922 [33,77]. The X paint FISH probe generated this way covers about 90% of the X. Adult
923 hermaphrodites were dissected on glass slides in 1x sperm salts and fixed in 4% PFA.
924 After 5 minutes of fixation, the specimen was covered with a 20x20 coverslip and placed
925 on dry ice for at least 20 minutes. The coverslip was then flicked off the slide with a
926 razor blade. Slides were washed in PBS-T three times and subjected to an ethanol
927 series of increasing concentrations (70%, 80%, 90%, 100% EtOH) for 2 minutes each,
928 after which the slides were air dried. To each slide, 10uL of X paint probe was added
929 and incubated at 37°C overnight. Next day, the slides were washed in a 39°C water
930 bath in 2x SSC/50% formamide three times, in 2X SSC solution three times for 5
931 minutes each, then in 1x SSC once for 10 minutes, followed by a room temperature
932 wash in 4x SSC. DAPI was included in the final 4x SSC wash and slides were mounted
933 using Vectashield. For FISH followed by IF, DAPI was excluded in the final 4X SSC
934 wash, after which IF was performed as described above.

935 Microscopy

936 Microscopy was performed using an Olympus BX61 microscope and a 60X APO oil
937 immersion objective. Images were taken with a Hamamatsu ORCA-ER High-Resolution
938 Monochrome Cooled CCD (IEEE 1394) camera. Images of nuclei were captured using
939 the Slidebook 5 program (Intelligent Imaging Innovations). Only nuclei with a clear
940 separation from the rest of tissue were imaged, no more than 3 per worm, and often no
941 more than 1. All experiments included imaging nuclei from at least three independent
942 experiments. A nucleus from the set 20 to 50 nuclei was chosen as a representiave
943 image. All representative images shown are maximum intensity projections of image
944 stacks taken with 0.2-micrometer Z-spacing. Quantification (see below) was performed
945 on the 3D stacks or individual Z planes, not on the maximum intensity projection
946 images. For images used for fluorescence intensity quantification, exposure times were
947 standardized to wild type. All images in the same type of analysis were then subjected
948 to identical min-max adjustments.

949 Quantification of signal intensity and signal enrichment

950 Fluorescence intensity of the DPY-27, CAPG-1, and H4K20me1 signals was quantified
951 in Slidebook 5. For each nucleus, the segment mask function was used to manually

952 capture the DAPI signal in 3D space and to create a DAPI mask. The mean
953 fluorescence for the appropriate channel (DPY-27, CAPG-1, H4K02me1) in the DAPI
954 mask in the 3D image stacks was recorded. This value was then divided by mean
955 fluorescence signal of the same channel in the same image in a region that represented
956 background fluorescence. Thus, the signal intensity represents mean signal intensity in
957 the nucleus/background intensity.

958 To quantify enrichment of the signal, the line intensity function was used in Slidebook on
959 a single Z plane from the middle of the nucleus. A line was drawn across the nucleus
960 including the enriched region (presumably the X chromosome). In nuclei with no clear
961 enrichment after DPY-27 depletion, a random line was drawn across the nucleus. The
962 peak signal intensity on the line-scan was divided by the lowest signal intensity to obtain
963 the ratio of relative enrichment of CAPG-1 or H4K20me1 on the X chromosomes over
964 the rest of the nucleus.

965 Quantification of X Volume

966 Z-stacked images of intestinal nuclei of hermaphrodites were trimmed to 10-15 slices at
967 to include only planes with nuclear signal. Background signal was subtracted in ImageJ
968 Fiji with a rolling ball radius of 50 pixels. After splitting the channels, the 3dManager
969 from the 3dSuite plugin was used to create a three-dimensional ROI of the DAPI signal
970 and a three-dimensional ROI of the FISH signal in the Cy3 channel [78]. For X volume
971 quantification, the area of the Cy3 channel ROI inside the DAPI ROI was then
972 compared in the 3dSuite 3DManager to find the X chromosome volume in the nucleus.
973 The mask for the X chromosomes was limited to the area that overlaps with the DAPI
974 mask signal, ensuring that the quantifications do not include non-specific staining of X
975 paint FISH. The proportion of the nucleus occupied by the X is a ratio of the X signal
976 volume to the DAPI signal volume measured in voxels (volumetric pixels).

977 Three-Zone Assay

978 From the images of nuclei stained using FISH targeting the X chromosome, the middle
979 slice with the most in-focus FISH signal was selected. The background was subtracted
980 in ImageJ FIJI with a rolling ball radius of 50 pixels. The DAPI and Cy3 channels were
981 then split and thresholded. Using the native ROI manager in ImageJ FIJI, the threshold
982 of the DAPI mask was used to draw three concentric ellipses that formed three zones of
983 equal area in the nucleus. The Cy3 signal overlap with each zone was calculated using
984 the ROI Manager to return the X chromosome FISH signal percentage in each zone.
985 For this assay, only nuclei with smooth edges and an elliptical shape were used.

986

987 mRNA-seq

988 Synchronized L1s were placed on HGM plates with or without auxin and NA22 [79]. 24-
989 hours later, L3 larvae were collected in M9. A small number of the larvae were removed
990 and allowed to grow to adulthood for control staining experiments to ensure complete
991 DPY-27 depletion. After pelleting, excess M9 was removed, and the remaining pellet

992 was snap-frozen in liquid nitrogen with 1mL of Trizol. RNA was extracted and cleaned
993 from the collected *C. elegans* using Qiagen RNeasy Kit. Reads were trimmed for quality
994 use. Poly-A enrichment, library prep, and next-generation sequencing were conducted
995 in the Advanced Genomics Core at the University of Michigan. RNA was assessed for
996 quality using the TapeStation or Bioanalyzer (Agilent). Samples with RINs (RNA
997 Integrity Numbers) of 8 or greater were subjected to Poly-A enrichment using the
998 NEBNext Poly(A) mRNA Magnetic Isolation Module (NEB catalog number E7490).
999 NEBNext Ultra II Directional RNA Library Prep Kit for Illumina (catalog number E7760L)
1000 and NEBNext Multiplex Oligos for Illumina Unique dual (catalog number E6448S) were
1001 then used for library prep. The mRNA was fragmented and copied into first-strand cDNA
1002 using reverse transcriptase and random primers. The 3' ends of the cDNA were then
1003 adenylated, and adapters were ligated. The PCR products were purified and enriched to
1004 create the final cDNA library. Qubit hsDNA (Thermofisher) and LabChip (Perkin Elmer)
1005 checked the final libraries for quality and quantity. The samples were pooled and
1006 sequenced on the Illumina NovaSeqX 10B paired-end 150bp, according to the
1007 manufacturer's recommended protocols. BCL Convert Conversion Software v4.0
1008 (Illumina) generated de-multiplexed Fastq files. The reads were trimmed using
1009 CutAdapt v2.3. FastQC v0.11.8 was used to ensure the quality of data [80,81]. Reads
1010 were mapped to the reference genome WBcel235 and read counts were generated
1011 using Salmon v1.9.0 [82]. Differential gene expression analysis was performed using
1012 DESeq2 v1.42.0 [83]. Downstream analyses were performed using R scripts and
1013 packages. For visualizing gene expression changes along chromosomes, log2 fold
1014 change data in each genotype comparison was displayed using the Chromomap
1015 package [84] after filtering for all reads at a significance level of $p<0.05$. Reads were
1016 positioned according to the chromosomal coordinates included in annotations provided
1017 by the reference genome in the previous RNAseq analysis and were displayed
1018 according to the *C. elegans* chromosome lengths found on WormBase.

1019 Supporting information

1020

1021 **S1 Fig. Unmodified original images for Fig 2. (A)** Unmodified original images of
1022 panels shown on Fig 2A. DPY-27 IF is shown in red, DNA stain (DAPI) in blue. **(B)**
1023 Unmodified original images of panels shown on Fig 2B. DPY-27 IF is shown in red, HTZ-
1024 1 IF in green (used as staining control) and DNA stain (DAPI) in blue. The main figure
1025 only shows that DPY-27 and DAPI color channels. Scale bars, 10 μm.

1026 **S2 Fig. Reproducibility of DPY-27 depletion.** Control non-auxin treated worms and
1027 worms treated with auxin from the L1 stage from 3 days, or from day 1 of adulthood for
1028 1 hr, or 24 hours were dissected and stain with anti-DPY-27 antibody, and anti-HTZ-1for
1029 staining control. Results from three independent experiments are shown. The merged
1030 images show DPY-27 in red and DNA (DAPI) in blue. Scale bars, 10 μm.

1031 **S3 Fig. Unmodified original images for panels shown on S2 Fig**. DPY-27 is shown
1032 in red, HTZ-1 (staining control) in green, and DNA (DAPI) in blue. Scale bars, 10 μm.

1033 **S4 Fig. Unmodified original images for panels shown on Fig 3**. **(A)** Unmodified
1034 images for Fig 3A. CAPG-1 staining is shown in green, H4K20me1 staining in red, DNA
1035 (DAPI) in blue. The main figure only shows the CAPG-1 and DAPI channels. **(B)**
1036 Unmodified images for Fig 3B. CAPG-1 staining is shown in green, HTZ-1 (staining
1037 control) in red, and DNA (DAPI) in blue. The main figure only shows the CAPG-1 and
1038 DAPI channels. Scale bars, 10 μm.

1039 **S5 Fig. Unmodified original images for panels shown on Fig 4**. **(A)** Unmodified
1040 images for Fig 4A. CAPG-1 staining is shown in green, H4K20me1 staining in red, DNA
1041 (DAPI) in blue. The main figure only shows the H4K20me1 and DAPI channels. **(B)**
1042 Unmodified images for Fig 4B. H4K20me1 staining is shown in green, HTZ-1 (staining
1043 control) in red, and DNA (DAPI) in blue. The main figure only shows the H4K20me1 and
1044 DAPI channels. Scale bars, 10 μm.

1045 **S6 Fig. Unmodified original images for panels shown on Fig 5**. X chromosome paint
1046 FISH probe is shown in red and DNA (DAPI) in blue. Scale bars, 10 μm.

1047 **S7 Fig. Comparison of all rings from the three-zone assay of X localization within**
1048 **the nucleus with and without auxin treatment.** (top) Three-zone assay for the X paint
1049 FISH signal in strains grown without auxin showing all three concentric zones. (Bottom)
1050 Three-zone assay for the X paint FISH signal in strains grown in the presence of auxin.
1051 Fig 5 shows only the data for the innermost zone.

1052 **S8 Fig. Analysis of *dpy-27::AID* RNA-seq samples. (A)** Principal component analysis
1053 (PCA) plot depicting the relationships among *TIR1; dpy-27::AID*, and *TIR1; dpy-27::AID;*
1054 *cec-4* with and without auxin treatment. **(B)** Unsupervised hierarchical clustering of
1055 *TIR1; dpy-27::AID*, and *TIR1; dpy-27::AID; cec-4* with and without auxin treatment using
1056 Manhattan distance to calculate distance between samples, and ward.D2 algorithm to
1057 cluster samples.

1058 **S9 Fig. Pearson correlation analysis of *dpy-27::AID* RNA-seq samples.** Heatmap
1059 represents color corresponding to the Pearson correlation coefficient between any two
1060 samples. Samples analyzed included the *TIR1; dpy-27::AID*, and *TIR1; dpy-27::AID;*
1061 *cec-4* strains with and without auxin treatment.

1062 **S10 Fig. Clustering analysis of all RNA-seq samples.** Unsupervised hierarchical
1063 clustering of all RNA-seq using Manhattan distance to calculate distance between
1064 samples, and ward.D2 algorithm to cluster samples.

1065 **S11 Fig. Pearson correlation analysis of all RNA-seq samples.** Heatmap represents
1066 color corresponding to the Pearson correlation coefficient between any two samples.

1067 **S12 Fig. mRNA-seq analysis of *dpy-27::AID* strains. (A-D)** Boxplots depicting the
1068 distribution of the expression difference of X-linked genes and expression difference of
1069 genes on autosomes. Gene expression is plotted as the log2 ratio of the strains being
1070 compared. Statistical significance is determined by the differences in gene expression
1071 between the X and autosomes by a Wilcoxon rank-sum test. Samples compared are
1072 shown above the boxplots (n.s. = not significant, * = $p < 0.05$, ** = $p<0.01$, *** = $p <$
1073 0.001).

1074 **S13 Fig. Chromomap analysis of gene expression change in strains with and**
1075 **without *cec-4* mutations. (A-D)** Log2 fold change in gene expression along the X
1076 chromosomes and autosomes. Samples compared are indicated above the maps.

1077 **S14 Fig. Unmodified original images for panels shown on Fig 7 and S15 Fig. (A)**
1078 Original unmodified images for Fig 7E. DPY-27 IF staining is shown in red and DNA
1079 (DAPI) in blue. **(B)** Original unmodified images for Fig S15. DPY-27 IF is shown in
1080 green, X chromosome paint FISH probe is shown in red and DNA (DAPI) in blue. Scale
1081 bars, 10 μm.

1082 **S15 Fig. DPY-27 localizes to the X chromosomes in *cec-4* and *dpy-21* mutants.**
1083 Signal for DPY-27 IF colocalizes with X-paint FISH signal. In the merged image, DPY-27
1084 is shown in blue and X paint FISH signal in red. DAPI is shown in grayscale. Scale bars,
1085 10 μm.

1086 **S16 Fig. RNA-seq analysis of *cec-4* and *dpy*-21 mutants. (A)** Principal component
1087 analysis (PCA) plot depicting the relationships among wild-type, single mutants (*cec-4*
1088 and *dpy-21*), and double mutants (*cec-4; dpy-21*) based on gene expression profiles.
1089 **(B)** Unsupervised hierarchical clustering of *cec-4* and *dpy-21* mutant RNA-seq datasets
1090 using Manhattan distance to calculate distance between samples, and ward.D2
1091 algorithm to cluster samples.

1092 **S17 Fig. Pearson correlation analysis of *cec-4* and *dpy*-21 mutant data sets.**
1093 Heatmap represents color corresponding to the Pearson correlation coefficient between
1094 any two samples.

1095 **S1 File. Numerical data and statistical analysis for Fig 1B.** Embryonic and larval
1096 viability after auxin exposure starting with the L4 stage of the parent. Total counts from
1097 three independent replicates are shown. Statistical analysis was performed using
1098 Fisher's exact tests. Statistically significant differences ($p<0.05$) are highlighted yellow.
1099 NA, not applicable

1100 **S2 File. Numerical data and statistical analysis for Fig 1E.** Survival of larvae
1101 exposed auxin from the L1 stage was quantified. Total counts from three independent
1102 experiments are shown. Statistical analysis was performed using Chi square tests.
1103 Statistically significant differences ($p<0.05$) are highlighted yellow.

1104 **S3 File. Numerical data and statistical analysis for Fig 2C.** Quantification of DPY-27
1105 fluorescence intensity. Statistical analysis was done using Brown-Forsythe and Welch
1106 ANOVA tests with multiple comparisons. Statistically significant differences ($p<0.01$) are
1107 highlighted yellow.

1108 **S4 File. Numerical data and statistical analysis for Fig 3C and D.** Quantification of
1109 CAPG-1 enrichment and fluorescence intensity. Statistical analysis was done using
1110 Brown-Forsythe and Welch ANOVA tests with multiple comparisons. Statistically
1111 significant differences ($p<0.05$) are highlighted yellow.

1112 **S5 File. Numerical data and statistical analysis for Fig 4C and D.** Quantification of
1113 H4K20me1 enrichment and fluorescence intensity. Statistical analysis was done using

Brown-Forsythe and Welch ANOVA tests with multiple comparisons. Statistically significant differences ($p<0.05$) are highlighted yellow.

S6 File. Numerical data and statistical analysis for Fig 5B. Analysis of X chromosome decondensation. Statistical analysis was done using Student's t-tests. Statistically significant differences ($p<0.05$) are highlighted yellow.

S7 File. Numerical data and statistical analysis for Fig 5C. Analysis of X chromosome localization within the nucleus via the three-zone assay. Statistical analysis was done using Student's t-tests. Statistically significant differences ($p<0.05$) are highlighted yellow.

S8 File. Statistical analysis of mRNA-seq. p values for the indicated comparisons are shown. Statistically significant differences ($p<0.05$) are highlighted yellow.

S9 File. Numerical data and statistical analysis for Fig 7A, B and C. Progeny viability in *dpy-21* and *cec-4* mutants. Average progeny counts from individual worms ($6<n<8$), collected over three independent experiments are shown. Statistical differences were evaluated using Student's t-tests. Statistically significant differences ($p<0.05$) are highlighted yellow.

S10 File. Numerical data and statistical analysis for Fig 7D. Analysis of X chromosome decondensation in *cec-4* and *dpy-21* mutants. Quantification of a total of 20 nuclei collected over the course of 3 to 4 independent experiments are shown. Statistical significance was evaluated using Student t-tests. Statistically significant differences ($p<0.05$) are highlighted yellow.

References

1. Ohno S. Sex Chromosomes and Sex-Linked Genes: Springer Berlin Heidelberg; 1967. doi:10.1007/978-3-642-88178-7

2. Lau AC, Csankovszki G. Balancing up and downregulation of the C. elegans X chromosomes. Curr Opin Genet Dev. 2015;31: 50–56. doi:10.1016/j.gde.2015.04.001

3. Madl JE, Herman RK. Polyploids and sex determination in Caenorhabditis elegans. Genetics. 1979;93: 393–402.

4. Nusbaum C, Meyer BJ. The Caenorhabditis Elegans Gene Sdc-2 Controls Sex Determination and Dosage Compensation in Xx Animals. Genetics. 1989;122: 579–593.

5. Hodgkin J. X chromosome dosage and gene expression in Caenorhabditis elegans: Two unusual dumpy genes. Mol Gen Genet. 1983;192: 452–458. doi:10.1007/BF00392190

1150 6. Meyer BJ, Casson LP. Caenorhabditis elegans compensates for the difference in X
1151 chromosome dosage between the sexes by regulating transcript levels. Cell.
1152 1986;47: 871–881. doi:10.1016/0092-8674(86)90802-0

1153 7. Hirano T. Condensins: organizing and segregating the genome. Curr Biol CB.
1154 2005;15: R265-275. doi:10.1016/j.cub.2005.03.037

1155 8. Ganji M, Shaltiel IA, Bisht S, Kim E, Kalichava A, Haering CH, et al. Real-time
1156 imaging of DNA loop extrusion by condensin. Science. 2018;360: 102–105.
1157 doi:10.1126/science.aar7831

1158 9. Kong M, Cutts EE, Pan D, Beuron F, Kaliyappan T, Xue C, et al. Human
1159 Condensin I and II Drive Extensive ATP-Dependent Compaction of Nucleosome-
1160 Bound DNA. Mol Cell. 2020;79: 99-114.e9. doi:10.1016/j.molcel.2020.04.026

1161 10. Hirano T. Condensins: universal organizers of chromosomes with diverse
1162 functions. Genes Dev. 2012;26: 1659–1678. doi:10.1101/gad.194746.112

1163 11. Csankovszki G, Collette K, Spahl K, Carey J, Snyder M, Petty E, et al. Three
1164 distinct condensin complexes control C. elegans chromosome dynamics. Curr Biol.
1165 2009;19: 9–19. doi:10.1016/j.cub.2008.12.006

1166 12. Mets DG, Meyer BJ. Condensins Regulate Meiotic DNA Break Distribution, thus
1167 Crossover Frequency, by Controlling Chromosome Structure. Cell. 2009;139: 73–
1168 86. doi:10.1016/j.cell.2009.07.035

1169 13. Hirano T, Kobayashi R, Hirano M. Condensins, chromosome condensation protein
1170 complexes containing XCAP-C, XCAP-E and a Xenopus homolog of the
1171 Drosophila Barren protein. Cell. 1997;89: 511–521. doi:10.1016/s0092-
1172 8674(00)80233-0

1173 14. Paul MR, Hochwagen A, Ercan S. Condensin action and compaction. Curr Genet.
1174 2019;65: 407–415. doi:10.1007/s00294-018-0899-4

1175 15. Chuang PT, Albertson DG, Meyer BJ. DPY-27:a chromosome condensation
1176 protein homolog that regulates C. elegans dosage compensation through
1177 association with the X chromosome. Cell. 1994;79: 459–474. doi:10.1016/0092-
1178 8674(94)90255-0

1179 16. Hagstrom KA, Holmes VF, Cozzarelli NR, Meyer BJ. C. elegans condensin
1180 promotes mitotic chromosome architecture, centromere organization, and sister
1181 chromatid segregation during mitosis and meiosis. Genes Dev. 2002;16: 729–742.
1182 doi:10.1101/gad.968302

1183 17. Lau AC, Nabeshima K, Csankovszki G. The C. elegans dosage compensation
1184 complex mediates interphase X chromosome compaction. Epigenetics Chromatin.
1185 2014;7: 31. doi:10.1186/1756-8935-7-31

1186 18. Lau AC, Csankovszki G. Condensin-mediated chromosome organization and gene
1187 regulation. Front Genet. 2014;5: 473. doi:10.3389/fgene.2014.00473

1188 19. Crane E, Bian Q, McCord RP, Lajoie BR, Wheeler BS, Ralston EJ, et al.
1189 Condensin-driven remodelling of X chromosome topology during dosage
1190 compensation. Nature. 2015;523: 240–244. doi:10.1038/nature14450

1191 20. Kim J, Jimenez DS, Ragipani B, Zhang B, Street LA, Kramer M, et al. Condensin
1192 DC loads and spreads from recruitment sites to create loop-anchored TADs in C.
1193 elegans. Tyler JK, editor. eLife. 2022;11: e68745. doi:10.7554/eLife.68745

1194 21. Chu DS, Dawes HE, Lieb JD, Chan RC, Kuo AF, Meyer BJ. A molecular link
1195 between gene-specific and chromosome-wide transcriptional repression. Genes
1196 Dev. 2002;16: 796–805. doi:10.1101/gad.972702

1197 22. Yonker SA, Meyer BJ. Recruitment of C. elegans dosage compensation proteins
1198 for gene-specific versus chromosome-wide repression. Development. 2003;130:
1199 6519–6532. doi:10.1242/dev.00886

1200 23. Pferdehirt RR, Meyer BJ. SUMOylation is essential for sex-specific assembly and
1201 function of the Caenorhabditis elegans dosage compensation complex on X
1202 chromosomes. Proc Natl Acad Sci. 2013;110: E3810–E3819.
1203 doi:10.1073/pnas.1315793110

1204 24. Kruesi WS, Core LJ, Waters CT, Lis JT, Meyer BJ. Condensin controls recruitment
1205 of RNA polymerase II to achieve nematode X-chromosome dosage compensation.
1206 Elife. 2013;2: e00808. doi:10.7554/eLife.00808

1207 25. Brejc K, Bian Q, Uzawa S, Wheeler BS, Anderson EC, King DS, et al. Dynamic
1208 Control of X Chromosome Conformation and Repression by a Histone H4K20
1209 Demethylase. Cell. 2017;171: 85-102.e23. doi:10.1016/j.cell.2017.07.041

1210 26. Wells MB, Snyder MJ, Custer LM, Csankovszki G. Caenorhabditis elegans dosage
1211 compensation regulates histone H4 chromatin state on X chromosomes. Mol Cell
1212 Biol. 2012;32: 1710–1719. doi:10.1128/MCB.06546-11

1213 27. Vielle A, Lang J, Dong Y, Ercan S, Kotwaliwale C, Rechtsteiner A, et al.
1214 H4K20me1 contributes to downregulation of X-linked genes for C. elegans dosage
1215 compensation. PLoS Genet. 2012;8: e1002933. doi:10.1371/journal.pgen.1002933

1216 28. Breimann L, Morao AK, Kim J, Sebastian Jimenez D, Maryn N, Bikkasani K, et al.
1217 The histone H4 lysine 20 demethylase DPY-21 regulates the dynamics of
1218 condensin DC binding. J Cell Sci. 2022;135: jcs258818. doi:10.1242/jcs.258818

1219 29. Kramer M, Kranz A-L, Su A, Winterkorn LH, Albritton SE, Ercan S. Developmental
1220 Dynamics of X-Chromosome Dosage Compensation by the DCC and H4K20me1
1221 in C. elegans. PLoS Genet. 2015;11: e1005698. doi:10.1371/journal.pgen.1005698

1222 30. Towbin BD, González-Aguilera C, Sack R, Gaidatzis D, Kalck V, Meister P, et al.
1223 Step-wise methylation of histone H3K9 positions heterochromatin at the nuclear
1224 periphery. Cell. 2012;150: 934–947. doi:10.1016/j.cell.2012.06.051

1225 31. Ikegami K, Egelhofer TA, Strome S, Lieb JD. Caenorhabditis elegans chromosome
1226 arms are anchored to the nuclear membrane via discontinuous association with
1227 LEM-2. Genome Biol. 2010;11: R120. doi:10.1186/gb-2010-11-12-r120

1228 32. Gonzalez-Sandoval A, Towbin BD, Kalck V, Cabianca DS, Gaidatzis D, Hauer MH,
1229 et al. Perinuclear Anchoring of H3K9-Methylated Chromatin Stabilizes Induced Cell
1230 Fate in C. elegans Embryos. Cell. 2015;163: 1333–1347.
1231 doi:10.1016/j.cell.2015.10.066

1232 33. Snyder MJ, Lau AC, Brouhard EA, Davis MB, Jiang J, Sifuentes MH, et al.
1233 Anchoring of Heterochromatin to the Nuclear Lamina Reinforces Dosage
1234 Compensation-Mediated Gene Repression. PLoS Genet. 2016;12: e1006341.
1235 doi:10.1371/journal.pgen.1006341

1236 34. Dawes HE, Berlin DS, Lapidus DM, Nusbaum C, Davis TL, Meyer BJ. Dosage
1237 compensation proteins targeted to X chromosomes by a determinant of
1238 hermaphrodite fate. Science. 1999;284: 1800–1804.

1239 35. Meyer BJ. Targeting X chromosomes for repression. Curr Opin Genet Dev.
1240 2010;20: 179–189. doi:10.1016/j.gde.2010.03.008

1241 36. Custer LM, Snyder MJ, Flegel K, Csankovszki G. The onset of C. elegans dosage
1242 compensation is linked to the loss of developmental plasticity. Dev Biol. 2014;385:
1243 279–290. doi:10.1016/j.ydbio.2013.11.001

1244 37. Yuzyuk T, Fakhouri THI, Kiefer J, Mango SE. The polycomb complex protein mes-
1245 2/E(z) promotes the transition from developmental plasticity to differentiation in C.
1246 elegans embryos. Dev Cell. 2009;16: 699–710. doi:10.1016/j.devcel.2009.03.008

1247 38. Sulston JE, Schierenberg E, White JG, Thomson JN. The embryonic cell lineage of
1248 the nematode Caenorhabditis elegans. Dev Biol. 1983;100: 64–119.
1249 doi:10.1016/0012-1606(83)90201-4

1250 39. Plenefisch JD, DeLong L, Meyer BJ. Genes that implement the hermaphrodite
1251 mode of dosage compensation in Caenorhabditis elegans. Genetics. 1989;121:
1252 57–76. doi:10.1093/genetics/121.1.57

1253 40. Cabianca DS, Muñoz-Jiménez C, Kalck V, Gaidatzis D, Padeken J, Seeber A, et
1254 al. Active chromatin marks drive spatial sequestration of heterochromatin in C.
1255 elegans nuclei. Nature. 2019;569: 734–739. doi:10.1038/s41586-019-1243-y

1256 41. Li Q, Kaur A, Mallory B, Hariri S, Engebrecht J. Inducible degradation of dosage
1257 compensation protein DPY-27 facilitates isolation of *Caenorhabditis elegans* males

1258 for molecular and biochemical analyses. Ward J, editor. G3
1259 GenesGenomesGenetics. 2022;12: jkac085. doi:10.1093/g3journal/jkac085

1260 42. Zhang L, Ward JD, Cheng Z, Dernburg AF. The auxin-inducible degradation (AID)
1261 system enables versatile conditional protein depletion in C. elegans. Development.
1262 2015;142: 4374–4384. doi:10.1242/dev.129635

1263 43. Hedgecock EM, White JG. Polyploid tissues in the nematode *Caenorhabditis*
1264 *elegans*. Dev Biol. 1985;107: 128–133. doi:10.1016/0012-1606(85)90381-1

1265 44. Kelly WG, Schaner CE, Dernburg AF, Lee M-H, Kim SK, Villeneuve AM, et al. X-
1266 chromosome silencing in the germline of C. elegans. Dev Camb Engl. 2002;129:
1267 479–492.

1268 45. Crittenden SL, Leonhard KA, Byrd DT, Kimble J. Cellular Analyses of the Mitotic
1269 Region in the Caenorhabditis elegans Adult Germ Line. Mol Biol Cell. 2006;17:
1270 3051–3061. doi:10.1091/mbc.E06-03-0170

1271 46. Schiksnis EC, Nicholson AL, Modena MS, Pule MN, Arribere JA, Pasquinelli AE.
1272 Auxin-independent depletion of degron-tagged proteins by TIR1. MicroPublication
1273 Biol. 2020: 10.17912/micropub.biology.000213.
1274 doi:10.17912/micropub.biology.000213

1275 47. Natsume T, Kiyomitsu T, Saga Y, Kanemaki MT. Rapid Protein Depletion in
1276 Human Cells by Auxin-Inducible Degron Tagging with Short Homology Donors.
1277 Cell Rep. 2016;15: 210–218. doi:10.1016/j.celrep.2016.03.001

1278 48. Martinez MA, Kinney BA, Medwig-Kinney TN, Ashley G, Ragle JM, Johnson L, et
1279 al. Rapid degradation of Caenorhabditis elegans proteins at single-cell resolution
1280 with a synthetic auxin. G3 Genes Genomes Genet. 2020;10: 267–280.

1281 49. Anderson EC, Frankino PA, Higuchi-Sanabria R, Yang Q, Bian Q, Podshivalova K,
1282 et al. X Chromosome Domain Architecture Regulates Caenorhabditis elegans
1283 Lifespan but Not Dosage Compensation. Dev Cell. 2019;51: 192-207.e6.
1284 doi:10.1016/j.devcel.2019.08.004

1285 50. Snyder MJ, Lau AC, Brouhard EA, Davis MB, Jiang J, Sifuentes MH, et al.
1286 Anchoring of Heterochromatin to the Nuclear Lamina Reinforces Dosage
1287 Compensation-Mediated Gene Repression. PLoS Genet. 2016;12: e1006341.
1288 doi:10.1371/journal.pgen.1006341

1289 51. Samejima K, Booth DG, Ogawa H, Paulson JR, Xie L, Watson CA, et al. Functional
1290 analysis after rapid degradation of condensins and 3D-EM reveals chromatin
1291 volume is uncoupled from chromosome architecture in mitosis. J Cell Sci.
1292 2018;131: jcs210187. doi:10.1242/jcs.210187

1293 52. Hirano T, Mitchison TJ. A heterodimeric coiled-coil protein required for mitotic
1294 chromosome condensation in vitro. Cell. 1994;79: 449–458. doi:10.1016/0092-
1295 8674(94)90254-2

1296 53. Houlard M, Godwin J, Metson J, Lee J, Hirano T, Nasmyth K. Condensin confers
1297 the longitudinal rigidity of chromosomes. Nat Cell Biol. 2015;17: 771–781.
1298 doi:10.1038/ncb3167

1299 54. Piskadlo E, Tavares A, Oliveira RA. Metaphase chromosome structure is
1300 dynamically maintained by condensin I-directed DNA (de)catenation. eLife. 2017;6:
1301 e26120. doi:10.7554/eLife.26120

1302 55. Zhiteneva A, Bonfiglio JJ, Makarov A, Colby T, Vagnarelli P, Schirmer EC, et al.
1303 Mitotic post-translational modifications of histones promote chromatin compaction
1304 in vitro. Open Biol. 2017;7: 170076. doi:10.1098/rsob.170076

1305 56. Corvalan AZ, Coller HA. Methylation of histone 4's lysine 20: a critical analysis of
1306 the state of the field. Physiol Genomics. 2021;53: 22–32.
1307 doi:10.1152/physiolgenomics.00128.2020

1308 57. Wilkins BJ, Rall NA, Ostwal Y, Kruitwagen T, Hiragami-Hamada K, Winkler M, et al.
1309 A cascade of histone modifications induces chromatin condensation in mitosis.
1310 Science. 2014;343: 77–80. doi:10.1126/science.1244508

1311 58. Javasky E, Shamir I, Gandhi S, Egri S, Sandler O, Rothbart SB, et al. Study of
1312 mitotic chromatin supports a model of bookmarking by histone modifications and
1313 reveals nucleosome deposition patterns. Genome Res. 2018;28: 1455–1466.
1314 doi:10.1101/gr.230300.117

1315 59. Das M, Semple JI, Haemmerli A, Volodkina V, Scotton J, Gitchev T, et al.
1316 Condensin I folds the Caenorhabditis elegans genome. Nat Genet. 2024;56: 1737–
1317 1749. doi:10.1038/s41588-024-01832-5

1318 60. Jans J, Gladden JM, Ralston EJ, Pickle CS, Michel AH, Pferdehirt RR, et al. A
1319 condensin-like dosage compensation complex acts at a distance to control
1320 expression throughout the genome. Genes Dev. 2009;23: 602–618.
1321 doi:10.1101/gad.1751109

1322 61. Kruesi WS, Core LJ, Waters CT, Lis JT, Meyer BJ. Condensin controls recruitment
1323 of RNA polymerase II to achieve nematode X-chromosome dosage compensation.
1324 Elife. 2013;2: e00808. doi:10.7554/eLife.00808

1325 62. Methot SP, Padeken J, Brancati G, Zeller P, Delaney CE, Gaidatzis D, et al.
1326 H3K9me selectively blocks transcription factor activity and ensures differentiated
1327 tissue integrity. Nat Cell Biol. 2021;23: 1163–1175. doi:10.1038/s41556-021-
1328 00776-w

1329 63. Csankovszki G, Panning B, Bates B, Pehrson JR, Jaenisch R. Conditional deletion
1330 of Xist disrupts histone macroH2A localization but not maintenance of X
1331 inactivation. Nat Genet. 1999;22: 323–324. doi:10.1038/11887

1332 64. Csankovszki G, Nagy A, Jaenisch R. Synergism of Xist RNA, DNA methylation,
1333 and histone hypoacetylation in maintaining X chromosome inactivation. J Cell Biol.
1334 2001;153: 773–783. doi:10.1083/jcb.153.4.773

1335 65. Heard E, Disteche CM. Dosage compensation in mammals: fine-tuning the
1336 expression of the X chromosome. Genes Dev. 2006;20: 1848–1867.
1337 doi:10.1101/gad.1422906

1338 66. Leonhardt H, Page AW, Weier HU, Bestor TH. A targeting sequence directs DNA
1339 methyltransferase to sites of DNA replication in mammalian nuclei. Cell. 1992;71:
1340 865–873. doi:10.1016/0092-8674(92)90561-p

1341 67. Audergon PNCB, Catania S, Kagansky A, Tong P, Shukla M, Pidoux AL, et al.
1342 Epigenetics. Restricted epigenetic inheritance of H3K9 methylation. Science.
1343 2015;348: 132–135. doi:10.1126/science.1260638

1344 68. Margueron R, Justin N, Ohno K, Sharpe ML, Son J, Drury III WJ, et al. Role of the
1345 polycomb protein EED in the propagation of repressive histone marks. Nature.
1346 2009;461: 762–767. doi:10.1038/nature08398

1347 69. Hansen KH, Bracken AP, Pasini D, Dietrich N, Gehani SS, Monrad A, et al. A
1348 model for transmission of the H3K27me3 epigenetic mark. Nat Cell Biol. 2008;10:
1349 1291–1300. doi:10.1038/ncb1787

1350 70. Liu W, Tanasa B, Tyurina OV, Zhou TY, Gassmann R, Liu WT, et al. PHF8
1351 mediates histone H4 lysine 20 demethylation events involved in cell cycle
1352 progression. Nature. 2010;466: 508–512. doi:10.1038/nature09272

1353 71. Brenner S. The genetics of Caenorhabditis elegans. Genetics. 1974;77: 71–94.

1354 72. Zhang S. Cell isolation and culture. WormBook. 2013; 1–39.
1355 doi:10.1895/wormbook.1.157.1

1356 73. Petty EL, Collette KS, Cohen AJ, Snyder MJ, Csankovszki G. Restricting dosage
1357 compensation complex binding to the X chromosomes by H2A.Z/HTZ-1. PLoS
1358 Genet. 2009;5: e1000699. doi:10.1371/journal.pgen.1000699

1359 74. Porta-de-la-Riva M, Fontrodona L, Villanueva A, Cerón J. Basic Caenorhabditis
1360 elegans Methods: Synchronization and Observation. J Vis Exp JoVE. 2012; 4019.
1361 doi:10.3791/4019

1362 75. M9 Buffer for Worms. Cold Spring Harb Protoc. 2014;2014: pdb.rec081315.
1363 doi:10.1101/pdb.rec081315

76. Ashley GE, Duong T, Levenson MT, Martinez MAQ, Johnson LC, Hibshman JD, et al. An expanded auxin-inducible degron toolkit for *Caenorhabditis elegans*. Greenstein D, editor. Genetics. 2021;217: iyab006. doi:10.1093/genetics/iyab006

77. Nabeshima K, Mlynarczyk-Evans S, Villeneuve AM. Chromosome Painting Reveals Asynaptic Full Alignment of Homologs and HIM-8–Dependent Remodeling of X Chromosome Territories during Caenorhabditis elegans Meiosis. PLoS Genet. 2011;7: e1002231. doi:10.1371/journal.pgen.1002231

78. Ollion J, Cochennec J, Loll F, Escudé C, Boudier T. TANGO: a generic tool for high-throughput 3D image analysis for studying nuclear organization. Bioinforma Oxf Engl. 2013;29: 1840–1841. doi:10.1093/bioinformatics/btt276

79. Zhang S, Kuhn JR. Cell isolation and culture. WormBook: The Online Review of C elegans Biology [Internet]. WormBook; 2018. Available: https://www.ncbi.nlm.nih.gov/books/NBK153594/

80. Martin M. Cutadapt removes adapter sequences from high-throughput sequencing reads. EMBnet.journal. 2011;17: 10–12. doi:10.14806/ej.17.1.200

81. FastQC. 2015. Available: https://qubeshub.org/resources/fastqc

82. Patro R, Duggal G, Love MI, Irizarry RA, Kingsford C. Salmon provides fast and bias-aware quantification of transcript expression. Nat Methods. 2017;14: 417–419. doi:10.1038/nmeth.4197

83. Love MI, Huber W, Anders S. Moderated estimation of fold change and dispersion for RNA-seq data with DESeq2. Genome Biol. 2014;15: 550. doi:10.1186/s13059-014-0550-8

84. Anand L, Rodriguez Lopez CM. ChromoMap: an R package for interactive visualization of multi-omics data and annotation of chromosomes. BMC Bioinformatics. 2022;23: 33. doi:10.1186/s12859-021-04556-z